The Report Committee for Stephen Matthew Kobdish certifies that this is the approved version of the following report:

MESH: A Maximum Power Point Tracker for a Wireless Sensor Network

APPROVED BY

SUPERVISING COMMITTEE:

Adnan Aziz, Supervisor

Jacob Abraham

MESH: A Maximum Power Point Tracker for a Wireless Sensor Network

by

Stephen Matthew Kobdish, B.S.E.E.

REPORT

Presented to the Faculty of the Graduate School of

The University of Texas at Austin

in Partial Fulfillment

of the Requirements

for the Degree of

Master of Science in Engineering

THE UNIVERSITY OF TEXAS AT AUSTIN

December 2010

To my family

Acknowledgments

I would like to acknowledge the valuable guidance received from my supervisor, Professor Adnan Aziz. I would also like to thank Professor Jacob Abraham for accepting to be the reader for this report at very short notice. Kudos also goes to my teammate Stephen Kobdish for providing his creativity, attention to detail, support throughout the project.

This work would not have been possible without the tremendous encouragement from my family, friends, coworkers, and fellow-students for the past two years.

MESH: A Maximum Power Point Tracker for a Wireless Sensor Network

Stephen Matthew Kobdish, M.S.E.
The University of Texas at Austin, 2010

Supervisor: Adnan Aziz

Energy harvesting is becoming increasingly important in low-power applications where energy from the environment is used to power the system alone, or to supplement a battery. For example, pulse oximeter sensors inside helmets of road racing cyclists are powered by the sun. These sensors have become smaller and more practical without the limitation of a finite energy supply. Harvested energy from an energy transducer (solar, piezoelectric, etc.) must be maximized to ensure these devices can survive periods where environmental energy is scarce.

The conversion process from the transducer to usable power for the device is not perfectly efficient. Specifically, the output voltage of a solar cell is a function of the light intensity, and by extension the load it powers. A small perturbation of the light source quickly diminishes the available power. The

wasted power reduces the energy available for the application, and can be improved using an approach called maximum power point tracking (MPPT). This technique maximizes harvesting efficiency by dynamically impedance matching the transducer to its load.

This report introduces the Maximum Efficient Solar Harvester (MESH), an MPPT algorithm tuned for a specific Wireless Sensor Network (WSN) application. MESH specifically controls the operation of the DC-DC converter in a solar power management unit (PMU). The control is done by monitoring the available light and feeding that information to choose the optimal operating point DC-DC converter. This operating point has a direct dependency on the overall efficiency of the system.

For MESH to be practical, the cost and power overhead of adding this functionality must be assessed. Empirical results indicate that MESH improves the maximum efficiency of the popular Texas Instruments (TI) RF2500-SEH WSN platform by an average of 20%, which far exceeds the power overhead it incurs. The cost is also found to be minimal, as WSN platforms already include a large portion of the hardware required to implement MESH.

The report was done in collaboration with Shahil Rais. It covers the hardware components and the bench automation environment; Rais's companion report focuses on software implementation and MESH architecture definition.

Table of Contents

List of Tables

List of Figures

Chapter 1

Introduction

1.1 Motivation

Solar powered applications, large and small, are becoming more pervasive in today's society where great emphasis is being placed on alternative energy sources. The use of photovoltaic (PV) cells take energy consuming systems off the grid, and provides a cleaner, and ideally, cheaper alternative to the traditional power company. However, solar power does not just benefit large energy consumers, but also devices in the μW range. WSNs using solar power can operate indefinitely without requiring battery replacement, and make applications like remote environmental monitoring feasible. Furthermore, designing out the battery, or reducing its size, improves the long-term cost of the Wireless Sensor Network (WSN) system, which is a high-priority requirement.

The amount of power a sensor node is able to harvest changes with the light intensity. In particular, the output voltage (V_{out}) of a solar panel varies with the intensity of light. The common technique used for increasing PV system efficiency is called maximum power point tracking (MPPT). This report presents an adaptation of an MPPT algorithm for Texas Instruments

(TI)'s RF-2500-SEH platform [17]. A hardware and software package called Maximum Efficient Solar Harvester (MESH) is developed as a supplement to the TI platform to improve its power efficiency. Boosting the solar conversion efficiency will not only help ensure the node can stay powered, but also helps with system cost since smaller cells and other hardware can shrink in size.

1.2 User Stories

MESH can be integrated into existing WSN solutions, or be designed into a new custom sensor application. Before implementing MESH several factors need to be considered in order to justify and adequately tune the MPPT algorithm for a given WSN application. The next section describes two real-world use cases, and gives insight into engineering and marketing requirements for implementing MESH.

1.2.1 Example Use Case: Joe the Farmer

The first example employes Joe the farmer. Farmer Joe would like to deploy a sustainable WSN in his field that will report vital crop data such as soil moisture, fertilizer content, and temperature back to the farmhouse. His field is large, and the number of sensors needed is also large. He needs his network to be sustainable, either running directly off of a solar cell, or a combination of solar cell and rechargeable battery. A power management system which can harvest the maximum amount of energy from a small solar cell must be developed to avoid the need for manual replacement of a battery.

For a field of size 100 acres Joe would like one sensor per acre to get a complete picture of his soil moisture situation. Joe likes to get updated data every one hour, and needs the data to be available even if it is night or during cloudy weather. When an update comes from the field each sensor on average needs to send a total of 5 transmissions depending on their configuration in the ad hoc mesh network. With a transmission power of 1.5mW Joe can get about 200 transmissions of 1ms each given a 100uAh battery, which is supplemented by a supercapacitor [14].

Assume that a company named S&S is created to market MESH, with a goal to reduce the cost of WSNs for their customers. S&S targets the solar panel, battery, and supercapacitors as components that will give the most cost reduction. Battery selection should be optimized for worst case lighting conditions. The addition of MESH allows the battery's size and cost to be reduced while still meeting the power requirements. The overhead cost of additional MPPT hardware is just that of a discrete MOSFET, one ceramic capacitor, and one resistor. These additional components total less than 10 cents when purchased in bulk [1], which is small compared to the cost of a larger battery. By using MPPT, Joe's system is able to receive less light and still keep the smaller battery charged for the soil updates.

1.2.2 Example Use Case: Sami the Marathon Coordinator

The second use case example employs Sami, the head of the health and safety team for the Austin Marathon. Sami is planning on providing each

runner with a device that attaches on to the runner's shoe lace. The device has a wearable solar panel and a tiny wireless sensor that tracks the runners vitals such as body temperature, location, and pulse. The solar panel provides power to the sensor to send the data back to Sami's base station. This allows Sami and the security team to monitor the vitals of each runner and deploy an emergency team to the location of runners who are on the verge of getting injured. It also allows Sami to ensure no runners have broken the marathon rules and offers a means for the marathon committee to ensure every runner has completed the race.

The marathon course is 26.2 miles long and covers an area of about 60 square miles. Base stations will be placed roughly one mile apart throughout the course at each water station to ensure no lapse in signal coverage. The sensors thrown on a random grid are capable of directing and organizing data flow to relay information back to the base station. On good sunlight conditions, the TI sensors are capable or relaying data as far as two miles given multi-hop between nodes [6], and can deliver 200 pulses of signal without sunlight. With a signal being relayed once a minute, a sensor platform can go more than half the marathon without the use of sunlight if power is managed correctly.

The system parameters described above can be used to decide sensor form factor and battery requirements. In this application the hardware size is extremely important since these devices will be worn by a runner. In this case the addition of MPPT can be used to reduce the size of a solar cell, battery, or remove it all together. MPPT has the ability to improve energy conversion

ratios such that cost, size, and useable life can be optimized.

1.3 Report Organization

Basic power management unit (PMU) architecture of a WSN node, benefits of adding MPPT, and details of how it is achieved is explained in Chapter 2. Chapter 3 covers the fine details of the MESH architecture, while Chapters 4 and 5 explains both the hardware and software components to implement MESH on the platform. Empirical results follow in Chapter 6. Once the baseline platform measurements have been determined, real time measurements with the inclusion of MESH are obtained to quantify its efficiency improvement in Chapters 7 and 8. Discussion of future work and some closing remarks are given in Chapter 9.

The contents of this masters report are the contributions of two authors, Shahil B. Rais, and Stephen Kobdish. Rais primarily covers the software implementation and MESH architecture definition in Chapters 3 and 5. Kobdish focuses on hardware and bench automation environment in Chapters 4 and 6.

Chapter 2

Basic Concepts

This section briefly touches on some concepts that are crucial to understanding how the MPPT solution works.

2.1 DC-DC Converters

The typical intelligent wireless sensor node is illustrated in Figure 2.1. A microcontroller (MCU) and radio frequency (RF) transceiver pair take in external data from sensors (e.g., light, temperature, acceleration) and puts this data out on a wireless network of other sensors. The MCU and RF transceiver usually run at a relatively higher voltage (1.8-3.6V) than the solar panel can output (0.8 - 1.5V). Between the solar panel and the MCU/RF pair is a DC-DC boost converter responsible for boosting the solar panel's output voltage to a level that can be used by the WSN. The DC-DC converter is part of the PMU sub-system, which regulates an energy storage device (e.g., battery, super-capacitor). This sub-system is the link between the low-voltage solar panel to the higher-voltage sensor node, and the focus of the discussed efficiency improvements.

There are two types of DC-DC converters used in sensor nodes: inductor-

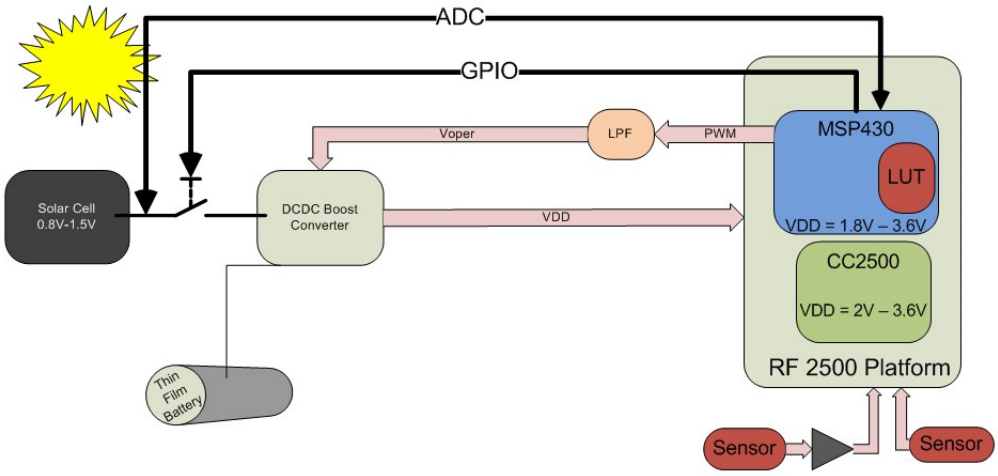

Figure 2.1: Typical wireless sensor node block diagram

based converters and switched-capacitor charged pumps [2]. This paper focuses on the former topology, though there is much overlap in the techniques employed in both.

The basic inductor-based DC-DC boost converter [4] is shown in Figure 2.2. The gate of the switching MOSFET is excited by a pulse width modulated (PWM) signal. When the transistor is turned ON, current flows directly through the inductor to ground and allows electrical energy to build up in the inductor's magnetic field. When the transistor returns to the OFF state the inductors magnetic field collapses and its stored energy is transferred to the output capacitor and load. For a boost converter, the output voltage at the load is greater than that at the input. The diode present prevents backlash current from propagating back to the inductor.

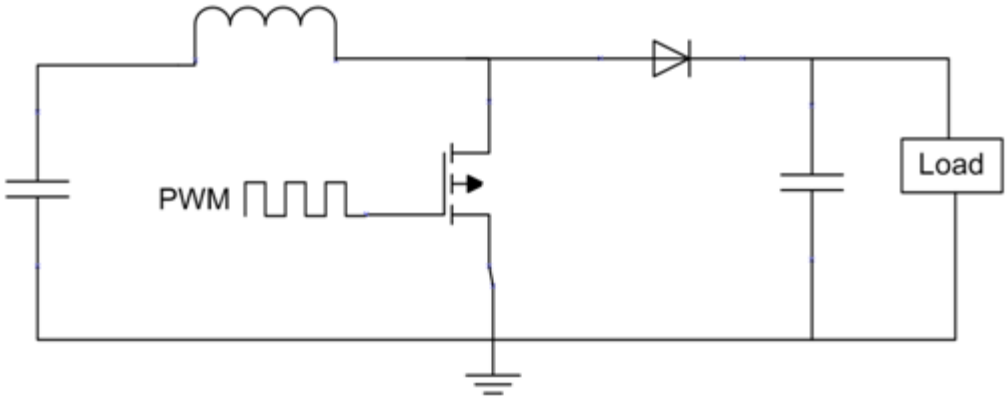

Figure 2.2: Basic Inductor Based DC-DC Converter

2.2 MPPT

MPPT directly affects the operation of a DC-DC converter, such as the one described in the previous section. MPPT is the control loop that feeds information about the system's input voltage to the PWM controller, which changes the duty cycle of the switching FET. The duty cycle can be dynamically varied to ensure delivery of optimum power from the solar cell. This concept can be thought as just impedance matching the input to the output of the converter based on environmental changes which affects the performance of the PV cell [2].

There are many MPPT implementations, including Perturb and Observe, Incremental Conductance, Open-circuit Voltage, and Short-circuit Current method [2]. These methods differ not only in logical process, but MPPT accuracy and cost as well. A small-scale MPPT scheme has to be tailored to

consume few MCU cycles in order to justify its place in the system's power budget. Furthermore, few additional hardware components should be added in order to address cost issues [14]. In his paper, Simjee et al. chose to implement the open-circuit MPPT because it is viewed as the most efficient choice for ultra-low-power applications [14]. This is because implementing the short circuit current method burns power while implementing MPPT, and accurately measuring current on chip is a more difficult than measuring voltage. Other MPPT methods also require too much power overhead to justify the increase in efficiency.

2.3 Open-Circuit Voltage Method

MPPT seeks to maximize output power of a PV cell by controlling the load it sees. The I-V plot of a typical solar panel is shown in Figure 2.3. On the I-V curve as the current draw increases the power delivered reaches a maximum point. As current is drawn beyond this maximum power-point the output voltage of the cell begins to drop rapidly and thus so does the delivered power. The goal is to maximize the time spent close to or at the point of maximum power transfer which yields maximum efficiency.

Environmental factors such as changes in light intensity by moving clouds or changes in temperature will cause many different I-V curves, each having their own maxima. An understanding of which I-V curve the system is currently operating on can be obtained by measuring the open-circuit voltage (V_{open}) of the solar cell [11]. This voltage gives an approximate correlation to

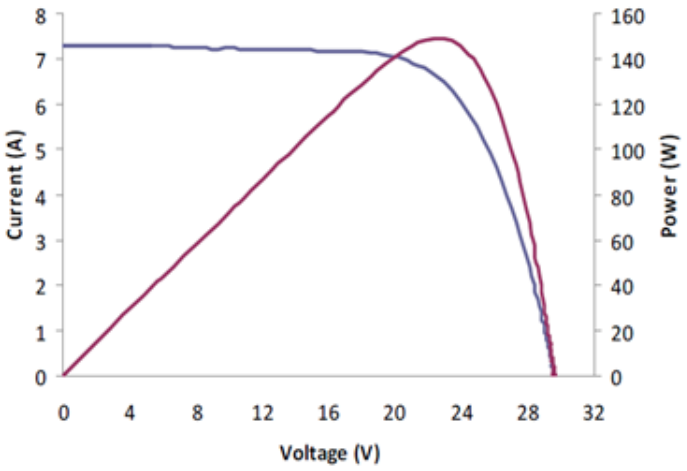

Figure 2.3: Typical Solar Panel I-V and P-V Plot. Power is maximized at the peak of the purple trace.

the cell under load.

The V_{open} MPPT method is achieved by reading the open-circuit voltage of the PV cell and using that information to control a DC-DC converter's PWM thus creating a feedback mechanism that compensates for light variation. The V_{open} method attempts to find the optimum point on the PV cell's I-V curve by tracking light-intensity only. Other MPPT schemes that take in additional inputs, such as temperature, are more accurate at finding the maximum power-point, but require additional power overhead that can outweigh the efficiency improvements in ultra low power applications. Based on the findings in [14] Simjee et al. were able to prove that V_{open} MPPT can be achieved with less than 5% tracking error, which is acceptable for a low power sensor.

Open circuit MPPT is easily achievable in most sensor platforms because an existing analog-to-digital converter (ADC) channel can be dedicated to measure the panel's open-circuit voltage, assuming it can be temporarily disconnected from the load. Additional inputs to the MPPT algorithm such as temperature or light intensity from a light sensor would help the system more closely hit its maximum power point. The use of additional sensor inputs will be explored in future work, but expect to find minimal efficiency improvement from the additional hardware, software, and power consumed to see minimal improvement [14].

Chapter 3

MESH Architecture

During the proof-of-concept phase, MESH was prototyped on the TI RF2500-SEH WSN development platform as described below. The MPPT implementation shown here is limited to the hardware and software modifications that could be made to optimize a pre-existing platform, the EZ430-RF2500. This portion of the research was completed by Rais. It is described in detail in his companion report [10], but is reproduced here for completeness.

3.1 EZ430-RF2500 Overview

The TI EZ430-RF2500 is a development board for evaluating both the MSP430 MCU and the CC2500 2.4GHz wireless RF transceiver [17]. An MCU and wireless radio is the core hardware of an intelligent WSN. The development kit is compatible with the IDE Kick Start software development environment and comes with a debugger for easy testing of the embedded code. It also comes with a solar panel sourced from Cymbet Corporation, along with a PMU that has two 50μAh thin film batteries (TFB). These TFB, called CBC5300, can be charged by the solar panel. This kit, shown in Figure 3.1, provides a starting point for an entire WSN or a generic MCU project. It was initially

used to model a realtime WSN in which audio streams were transferred from one device to another. This work was the result of two class projects [6], and provided a basis for this project in wireless sensors. Here, improvements are made to the existing platform design to optimize the power efficiency.

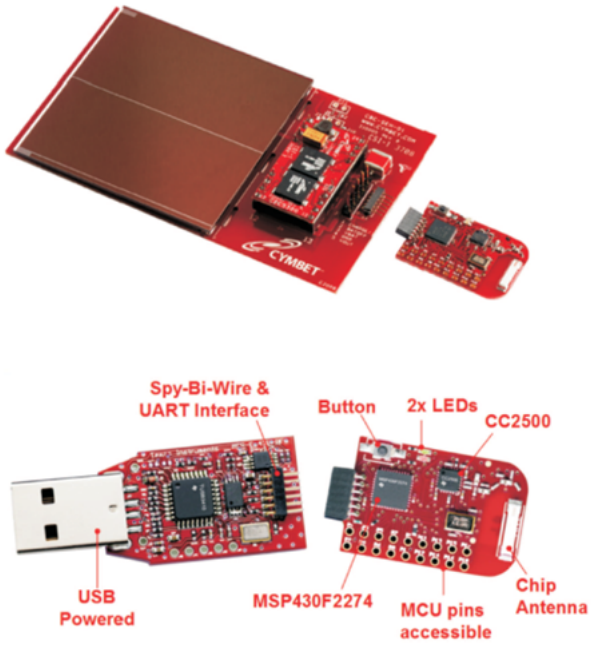

Figure 3.1: Solar Energy Harvester TI Platform [17].

3.2 Platform Features

Coupling MESH and the TI WSN kit has several advantages For instance, it combines the use of a solar energy transducer with an efficient power module to translate light energy to useful electrical energy that can either be stored or directed at an application. Typical solar cells produce low voltages

in the range of 1.0V; thus, a boost converter is used to produce a more useful voltage of approximately 3.6V to power the end application and charge the TFB. With flexibility in mind, the PMU is capable of accepting other energy transducer inputs such as piezoelectric and thermoelectric. The overall platform uses the transducer input to store harvested power and intelligently deliver managed power to a target application while ensuring power efficiency is optimized for all given input conditions.

The platform also implements many power saving features. For example, the charge control block continuously monitors V_{out} of the boost converter to ensure it is high enough to provide stable power to the end device. If it does not meet the V_{oper}>$3V$ threshold, the boost circuit is disconnected from the output to prevent the TFB from dumping its energy back into the converter. In addition, there are control signals present to ensure the TFB does not get a deep discharge in low light or high load situations. Deep discharge is a condition where a battery is drained to less than 5% of its full capacity. The TFB's lifetime is heavily dependent on the rate of discharge and is severely shortened if it drops below 50% [3]. To mitigate this, charge control and battery signals are present to allow the MCU to dictate how and when the battery is charged, or to completely disallow the TFB from powering the end application [3]. These signals ultimately preserve battery life in a prolonged low light condition. The PMU also ensures that the target application is safely powered on with a slow and smooth transition from zero to full-scale voltage V_{reg}.

3.3 MESH Control Variable Descriptions

MESH is accomplished by using several control signals to implement the MPPT functionality. For example, the solar disconnect pin on the CBC5300 is driven high to disconnect the load from the PV [3]. This then allows MESH to measure V_{open} with no load attached. This voltage reading is then relayed to the LUT to determine the ideal V_{oper}.

A PWM and DAC can both be used to drive V_{oper}. This signal feeds into an amplifier feedback circuit in the PMU, which forces the PV cell voltage V_{solar} to track with it when no load is connected. V_{solar} also tracks with sunlight and is independent of the output load placed on the platform. This allows MESH to optimize the circuit without dependency on the end application. Because the feedback amplifier is present V_{oper} also controls I_{solar}, the amount of current produced by the PV cell. Like V_{solar}, it is highly dependent on light intensity and it's direct load, the PMU.

With MESH connected, the PMU is capable of producing $V_{out} = 3.6V$ and can pull roughly $30\mu A$ at 3V at steady state, a sizeable load in low power applications. Additional capacitors at the load account for the short bursts of high current pulses required by the end circuit.

The platform efficiency η_o is calculated by the ratio of the power consumed at the output of the PMU to the power generated by the solar panel for a given light and load condition:

$$\eta_o = \frac{P_{output}}{P_{solar} + P_{MESH}} \tag{3.1}$$

where P_{output} is the power being delivered to the load, P_{solar} is the power consumed by the solar panel, and P_{MESH} is the power consumed by the MESH circuitry.

The goal is to maximize this efficiency η_o during the power transfer from the solar panel to the output of the PMU. The platform power now incorporates newly added devices such as the DAC, PWM, and the switch. In an ideal condition, the power overhead of adding these components should not outweigh the efficiency improvements of MESH.

3.4 V_{open} and I_{short} Measurements

Two good MPPT solutions discussed in [14] use a switch to disconnect or short the PMU from the solar panel to either measure V_{open} or the short circuit current I_{short}. The correlation between these parameters is measured and shown in Figure 3.2.

Each datapoint on the plot represents a unique light condition, with the point closest to the origin representing the darkest light condition. The curve exhibits a hyperbolic relationship between V_{open} and I_{short}. It approaches an asymptote at 1.5V for the voltage and 0A for the current as expected. The PV's built-in circuit disallows from placing a short on the PV as it would eventually damage the cells [3]. Thus, the open circuit voltage will be exploited as a baseline for characterizing the panel.

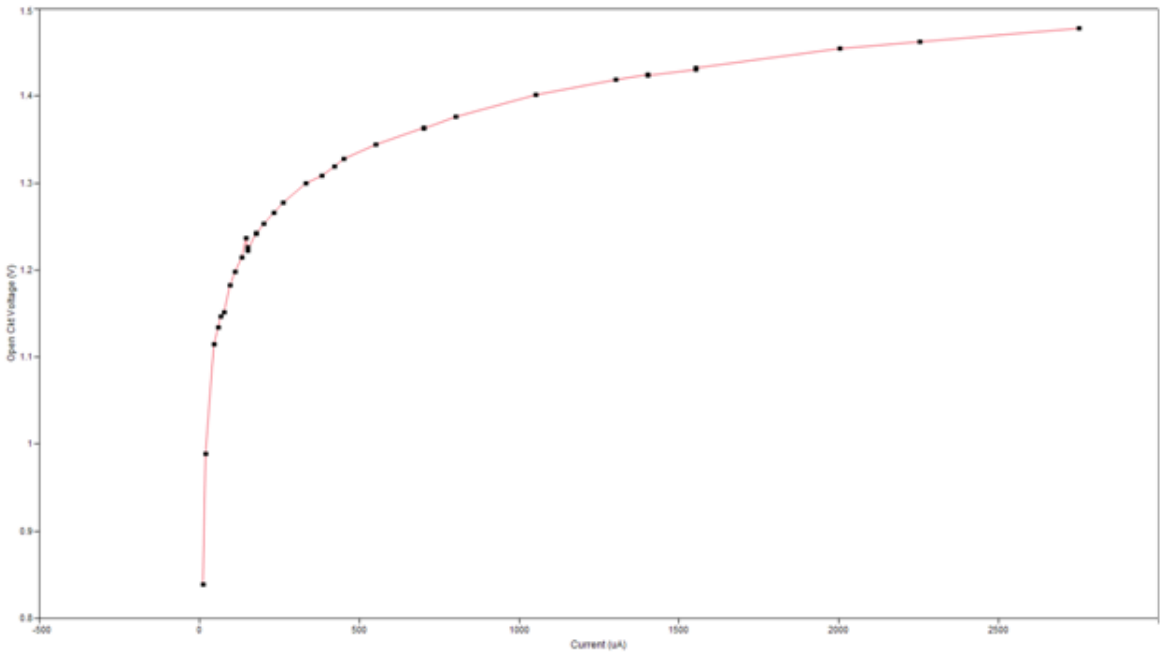

Figure 3.2: Relationship between V_{open} and $I_{short}$of PV panel

3.5 V_{open} Correlation to Light Source

V_{open} also has a correlation to the light source. Figure 3.3 shows the near linear relationship between the open circuit panel voltage and the light source. The light source is measured as the number of A4 sheets placed on a light source, and not in lumens. Higher numbers indicate a lower light condition.

The X-axis represents the sheets of papers placed on the light source to mask the light trajectory. A decreasing light source reduces the open circuit voltage on the panel. The last two points should be omitted as the PV starts

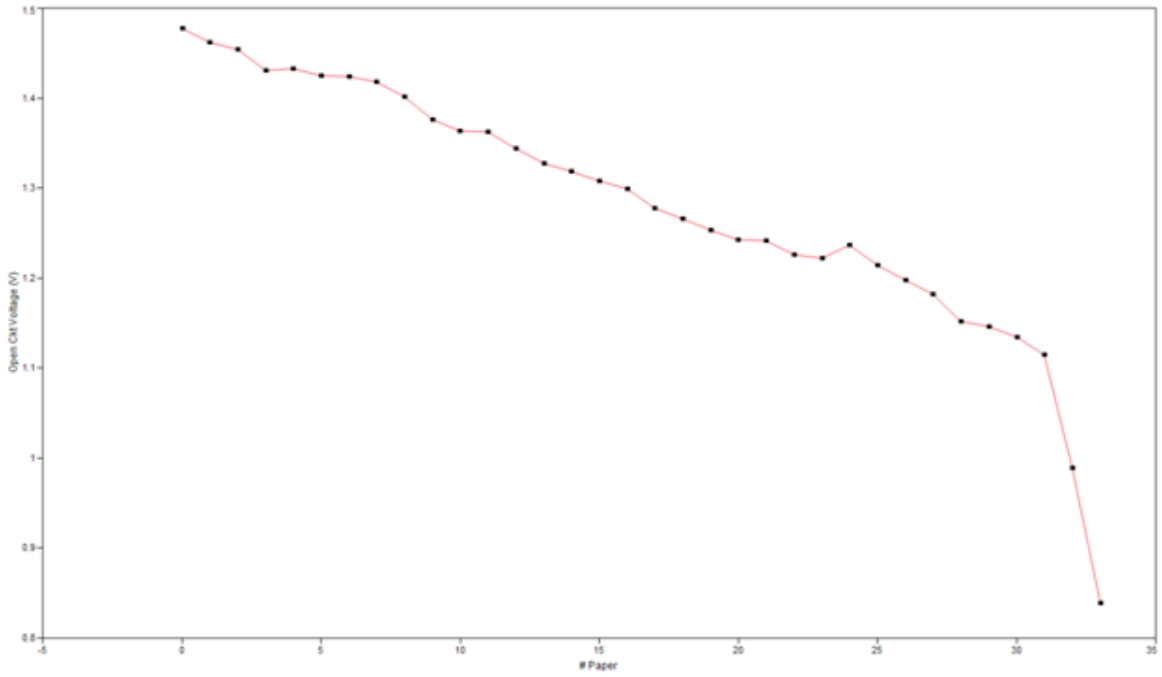

Figure 3.3: Relationship between open circuit voltage and the light source of PV panel

to saturate to 0.7V as the light source is drastically reduced.

3.6 PMU Characteristics

The PMU is compatible with many types of transducers to provide the end user flexibility to select the harvester that best meets the design goals. Because of the flexibility in design, one possible issue is the impedance mismatches between the transducer's output and the PMU's input. A poorly matched transducer violates the MPPT theory and thus becomes inefficient. The PMU can accept an output impedance range of 58Ω to 4kΩ with an in-

put voltage from 300mV to 1.5V, with at least 700mV open circuit voltage to kickstart the operation [3].

Peak efficiency will occur at a nominal transducer input voltage of 800mV to 1.0V at 1kΩ. Operating characteristics for most transducer types are typically available from the datasheet. The PV operating curve as measured and used in this project is shown in Figure 3.4.

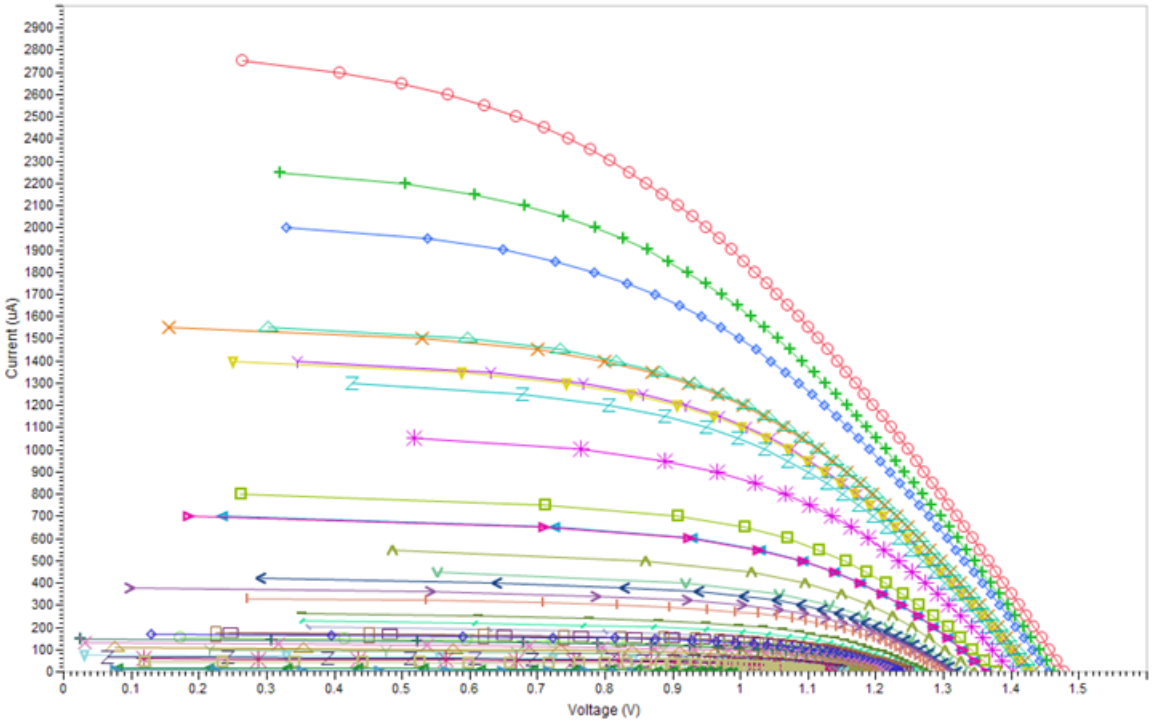

Figure 3.4: Relationship between the current draw and the resulting voltage on the PV panel

Output impedance, operating voltage, and peak power point can also be verified by empirical measurements. This can be done by measuring the

load voltage and current as the load impedance across the transducer is swept. The range swept must be broad enough to cover the peak power point. This peak is the maximum product of the measured load voltage and current.

3.7 V_{oper} Control

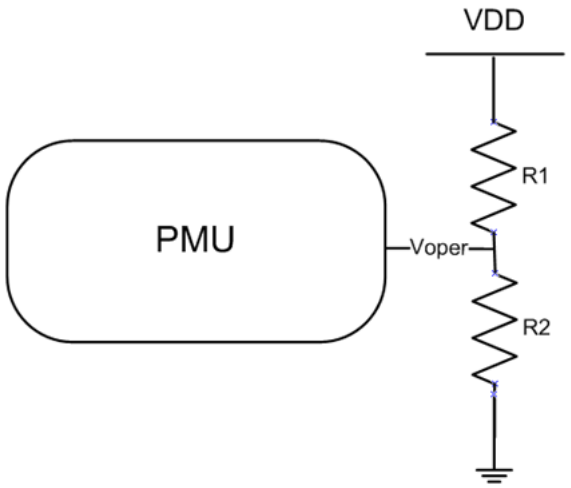

Figure 3.5: Solar Energy Harvester TI Platform [17].

Once the optimal operating point is discovered (either through the datasheet or empirical measurements), the operating point V_{oper} is traditionally set using a voltage divider as shown in Figure 3.5. The voltage divider is supplied by the full-scale voltage V_{reg}. The resulting V_{oper} is calculated by:

$$V_{oper} = V_{reg} \frac{R_2}{R_1 + R_2} \tag{3.2}$$

where V_{reg} is nominally 4.06V and R_2 is in the range of 500kΩ to 1MΩ. The optimal R_2 value is 750kΩ [3] to provide low input ripple voltage.

A more useful formula is to determine R_1 given all the other variables:

$$R_1 = R_2 \cdot \left(\frac{V_{reg}}{V_{oper}} - 1 \right) \tag{3.3}$$

For example, for a 1MΩ PV with an operating voltage of 1.01V, R_1 can be determined as:

$$R_1 = 1M\Omega \cdot \left(\frac{4.06V}{1.01V} - 1 \right) = 3.02M\Omega \tag{3.4}$$

A 3.01MΩ resistor is the nearest standard value that can be used. R_2 was chosen as a standard resistor value of 1MΩ; 750kΩ, another standard resistor value, can also be used for R_2 but will result in a V_{oper} that is farther away from the nominal value due to the standard values available. Thus, there is a tradeoff between efficiency and signal-to-noise ratio (SNR) depending on the resistor value chosen.

A capacitor is also used at the output to set the bandwidth of the boost converter control loop. If a low impedance transducer is used, this capacitor would have to be reduced in value to accommodate a lower bandwidth. The ideal bandwidth can be easily chosen by probing a gate pin on the CBC5300 to ensure the amplifier is still in saturation [3].

It quickly becomes obvious that setting static values for V_{oper} drastically reduces the platform efficiency if the end circuit is not operating at the ideal peak power point. This is because the platform becomes poorly matched to the transducer. The luxury of dynamically varying V_{oper} (either using the DAC or PWM) is thus critical to improving overall efficiency.

Chapter 4

MESH Hardware Implementation

This chapter outlines the actual hardware modifications that were made to the RF-2500-SEH platform in order to implement the MPPT solution.

4.1 Hardware Optimization

Setting V_{oper} dynamically is not an easy task. Several field measurements where required to baseline the optimum working load of the solar panel over different light conditions.

The MPPT subsystem requires that hardware be added to the RF2500 platform. As explained in the previous chapter, the additional hardware functions include disconnecting the panel from the system, sampling the panel voltage through an ADC, and supplying the DC V_{oper} signal which controls the operating point of the DC-DC converter. Any additional hardware added to the solar power management unit requires it's power overhead to be carefully quantified.

The MPPT solution itself cannot consume more power than it is saving for a given period of time; otherwise it is counterproductive. It may be acceptable if instantaneous spikes in power exceed the average budget long as

the average integral power is less than the power saved. A generic example of this is illustrated in Figure 4.1.

Suppose rough estimates from the platform show that the solar panel is supplying 200μW under static conditions and in steady-state. The PMU hardware is only delivering 60μW in steady-state or is 30% efficient. Thus, this sets the baseline for the power budget. Then, the MPPT's average power cannot exceed this 60μW to satisfy equilibrium. Notice, however, that periodic power spikes from accessing MPPT can exceed the power budget as long as the average over time is still constrained within the 60μW. More frequent power surges will eventually blow the average power budget, which will make the MPPT ineffective. To mitigate this, the rate at which MPPT is serviced can be reduced.

4.2 Switch

In order to measure the V_{open} the power from the solar cell must be temporarily removed from the rest of the PMU system. Disconnecting the panel in the current platform is not trivial using discrete MOSFETs. The low-voltage panel does not create a large enough V_{ds} to be switched using a typical CMOS general purpose I/O (GPIO) voltage (about 3.3V). Once it was realized that a discrete solution was impractical, an off-the-shelf Fairchild analog switch was purchased [5]. The FSA1156 analog switch is similar to a standard relay except that it has no mechanical parts. This switch takes a standard CMOS input as control and will pass any voltage between ground

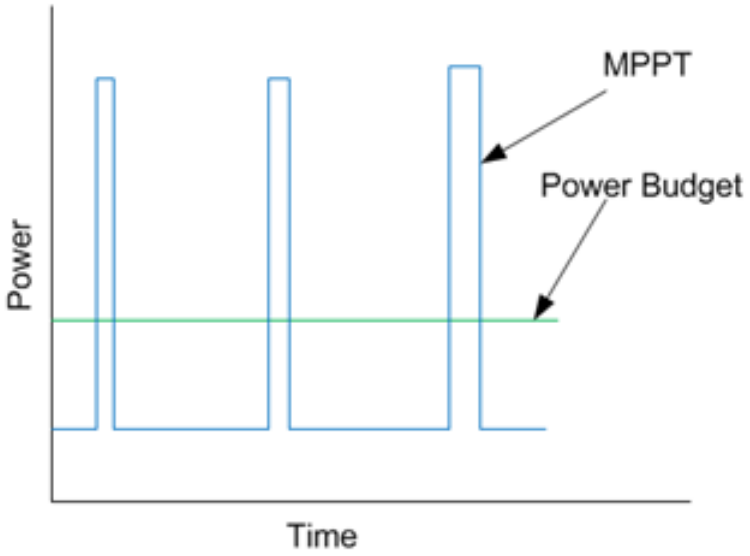

Figure 4.1: Average of peak power condition over time must not exceed power budget. This can be implemented by spacing peak power levels through software.

and the supply rail. A GPIO from the MSP430 is used to open the switch during the V_{open} collection phase. The on-resistance (r_{ON}) of the device must be accounted for to ensure the MPPT budget is met. The r_{ON} resistance is typically extremely low at $< 1\Omega$ [5], so the power burned by the switch is:

$$\begin{aligned} P_{switch} &= P_{r_{ON}} + P_{leakage} \\ &= (I_{solar})^2 \cdot r_{ON} + (I_{leakage}) \cdot V_{reg} \\ &= (1mA)^2 \cdot (1\Omega) + (1\mu A) \cdot (3.6V) \\ &= 5\mu W \end{aligned} \tag{4.1}$$

at peak. This amount of extra burned power may hurt our MPPT budget, but during the proof-of-concept phase is acceptable.

4.3 The V_{oper} Input

As previously described, the current design of the CBC5300 uses a static resistor divider to set an optimum V_{oper}. This signal varies an internal PWM in the CBC5300 that dictates the efficiency of the platform in terms of solar power converted to usable power for the WSN. The resistor divider values are chosen given optimistic baseline conditions that assumes a given load with a given lighting condition. In other words peak efficiency will only be achieved if the WSN can mimic this specific condition, which will is unrealistic given the myriad of operating conditions. Moreover, efficiency quickly diminishes when the ideal conditions are not satisfied, resulting in large efficiency dropouts on the platform as a whole.

The V_{oper} input to the CBC5300 is a static DC voltage that sets the DC-DC converter's optimal working point [3]. To improve the efficiency of the platform, a simple way to vary V_{oper} was required. This programmable DC voltage source must have low-power overhead as well as be continuously supplied to the V_{oper} pin since the resistor dividers will be eliminated. The methods explored to produce V_{oper} included a programmable resistor divider by using a digital potentiometer, a PWM passed through a low-pass filter (LPF), and using a digital to analog converter (DAC). All of these solutions produced peak powers far exceeding the MESH budget, and techniques to

overcome this problem will be discussed in later sections

4.4 DAC

One method of generating V_{oper} that was explored was to use an external DAC controlled by the MSP430. The TI 5571 8-bit DAC communicates with the MSP430 over the I2C protocol, as shown in Figure 4.2 [15]. Once the proper I2C drivers were implemented this solution offered a reliable, stable, and scalable method. It also more closely mimics the original plan of using the MSP430's integrated DAC.

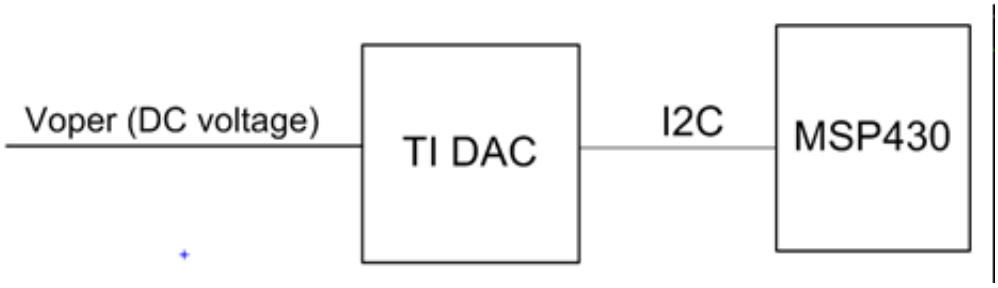

Figure 4.2: DAC connection to MSP430 using I2C

4.5 PWM

The MSP430 also provides a method of generating a PWM signal through the tick-timer module. The timer can be setup to modulate the high and low time of a GPIO thus achieving a PWM signal. The proposal to generate V_{oper} involved passing the MSP430s PWM signal though a LPF consisting of a simple resistor and capacitor, as shown in Figure 4.3

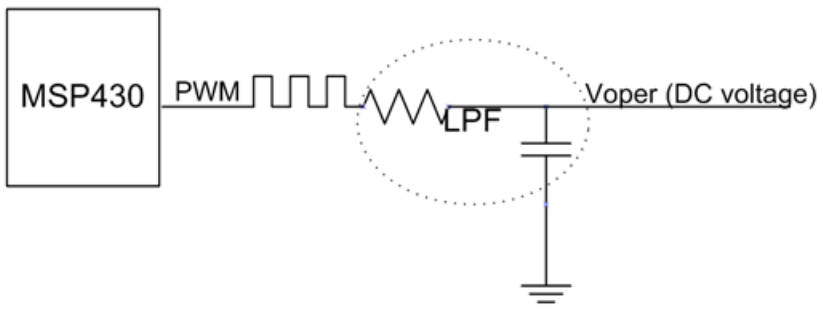

Figure 4.3: PWM and LPF circuitry shown being applied to V_{oper}

The authors have had experience with this technique in previous projects, and were able to simulate the response of this solution before implementing it in actual hardware and software, as in Figure 4.4. Some concerns about power consumption and overhead, voltage stability, and system response were raised early in the planning by the advisor. These concerns are mitigated in later sections.

4.6 Selection Criteria for V_{oper} Control

The initial plan involved using the integrated DAC on the MSP430 as a solution to generate V_{oper}. This method required no additional hardware except for a wire bus between the MSP430 MCU and the V_{oper} input pin. After more investigation, the discovered that the MCU package used in the RF2500 platform did not support pinouts for the DAC. While functionality was present, the DAC was omitted by TI to lower costs. With the integrated DAC no longer being an option, the solution requiring the least amount of

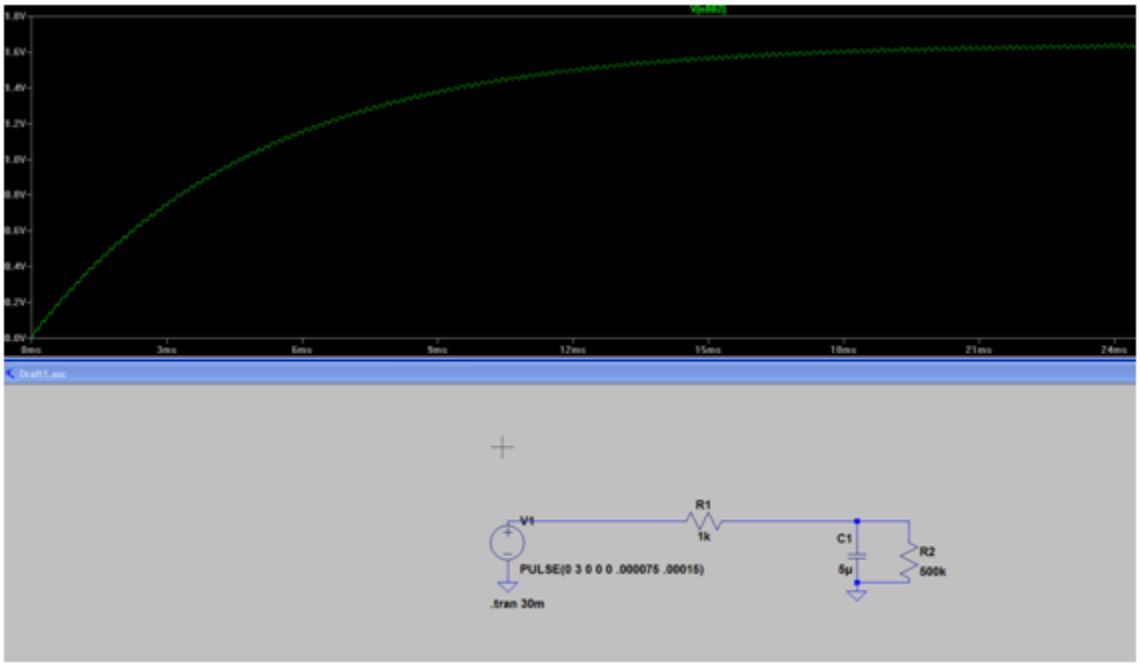

Figure 4.4: Simulation environment for proof of concept PWM solution.

external hardware was chosen. The method selected was using the PWM piped through a LPF.

Chapter 5

Software Design and Integration

This section discusses the software written to support MESH. The full annotated C-code is available in [9]. This portion of the research was completed by Rais. It is described in detail in his companion report [10], but is reproduced here for completeness

5.1 Software Overview

One of the main goals when developing MESH was to implement the solution on a real system running a practical application. Using MESH in a real system gives it credibility and helps gain confidence that it could be suitable for pervasive use. The software stack of this MPPT solution has been integrated in two example applications.

The first is TI's example demo for WSNs. This demo application establishes a star network topology consisting of a single access point (AP) and up to five end devices (ED). These EDs collect several sets of datapoints and transmits it back to the AP. The data collected includes temperature (using the internal temperature diode in MSP430) and the battery voltage rail (V_{bat}) both using the ADC. This information is then logged and displayed by the AP

on screen.

The second application is a WSN implemented using the existing platform developed by the authors. It uses the same development kit to stream continuous music waves to the AP using the SimpliciTI© network protocol. The data was transmitted from the ED to AP using multihop, a method that wisely chooses the path of least power to transmit data. The application design took into consideration factors such as modulation schemes, PATABLE power, filter bandwidth, power sensitivity, and datarate [6]. This application was developed by the authors for a related class and served as a realistic application base to test and demonstrate the features of MESH.

5.2 MESH Integration in Example Applications

As in most WSNs or well-designed embedded systems, the devices are put into a low-power state as often as possible. The ED can enter a mode which shuts down most of the systems clocks and peripherals consuming only 10μA in standby mode. Multiple interrupt sources can be used to wake the system up and perform various tasks. For example both applications wake up the MCU to establish the radio link and transmit sensor data.

MESH was implemented as an additional interrupt source with a tunable frequency. Being able to control the frequency of performing MESH updates allows for a design variable that can be tweaked to meet the needs of many applications each with their own power needs. In this example MESH is iterated every five seconds to provide balance between power overhead and

efficiency improvement. In the field, this time interval is considered an overkill given WSN applications do not need to be refreshed this often. For example, Joe the farmer would only need crop data once an hour at most, or Sami from the marathon example would only need to get runner's information every few minutes.

5.3 Software Design Flow

The software design flow of the code is illustrated in Figure 5.1. When the MESH code is executed the CPU is brought out of sleep and the V_{oper} output is sent to the CBC5300. The solar panel is then disconnected from the system when a GPIO cuts off the analog switch. The sensor's ADC is enabled to acquire the V_{open} voltage measurement at the output of the panel. Enabling the ADC actually provides another chance for the MSP430 to be put to sleep. The system allows for entering an ultra low power mode while waiting for an interrupt signaling an acquisition has completed [16].

The result of the ADC acquisition is used to index a dictionary of V_{open} readings to PWM frequencies. Once the necessary change in frequency is determined the PWM modulates, resulting in a DC change at the V_{oper} input. The 5kHz PWM signal is generated by programming the MSP430's timer registers appropriately. The frequency of the PWM is chosen to be fixed, but the duty-cycle is controllable and dynamically controlled according to changes in the panels V_{open} voltage.

The algorithm just described implements the intelligence behind the

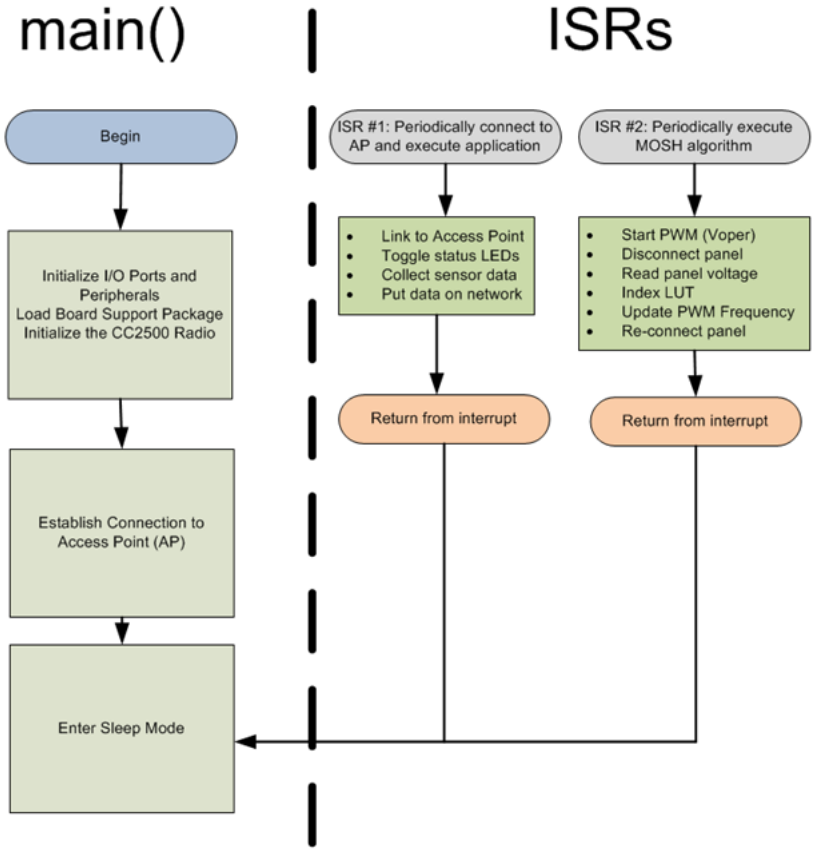

Figure 5.1: Code flow diagram illustrating main() along with the interrupt service routines (ISR)

feedback method used in MESH. Many of these software parameters such as interrupt frequency, PWM duty cycle, and LUT step-size granularity are key in adapting MESH to many different WSN applications. The light weight 500-line code is easy to implement in existing WSN applications. Challenges include integration of MESH onto example platforms, redefining interrupt and timing parameters on existing code stacks, and simultaneously debugging hardware

and software components. The final code took roughly five weeks to develop and debug to a fully working condition.

Chapter 6

Experimental Characterization of MESH

Generating the LUT is an important factor to implement an efficient MPPT algorithm. Creating the V_{open} LUT can be achieved through simulation, empirical data collection, or both. The system chosen is based on empirical measurements on the platform since writing accurate simulation models would be time prohibitive and would add little if any value over actual system characterization.

The empirical measurements method involves measuring and supplying a few simple parameters listed in Table 6.1.

Table 6.1: Measurement Variables and Descriptions

#	Variable	Description
1	V_{oper}	DC-DC control input
2	V_{solar}	PV voltage when connected
3	I_{solar}	PV current to CBC5300
4	I_{src}	Controlled Output current
5	I_{out}	Output current of CBC5300
6	V_{out}	Output voltage of CBC5300
7	V_{open}	Open-circuit PV voltage

These variables can be monitored and studied to determine the ideal set of conditions for the overall platform. Software and hardware optimizations

can be performed based on these ideal conditions to ensure the platform is always operating within the ideal boundary.

6.1 Measurement Automation

The solar panel must be thoroughly characterized under various light conditions and DC-DC converter loads to populate an accurate software LUT. This LUT associates an open-circuit panel voltage V_{open} with a feedback operating voltage V_{oper} inputted to the DC-DC converter on the CBC5300.

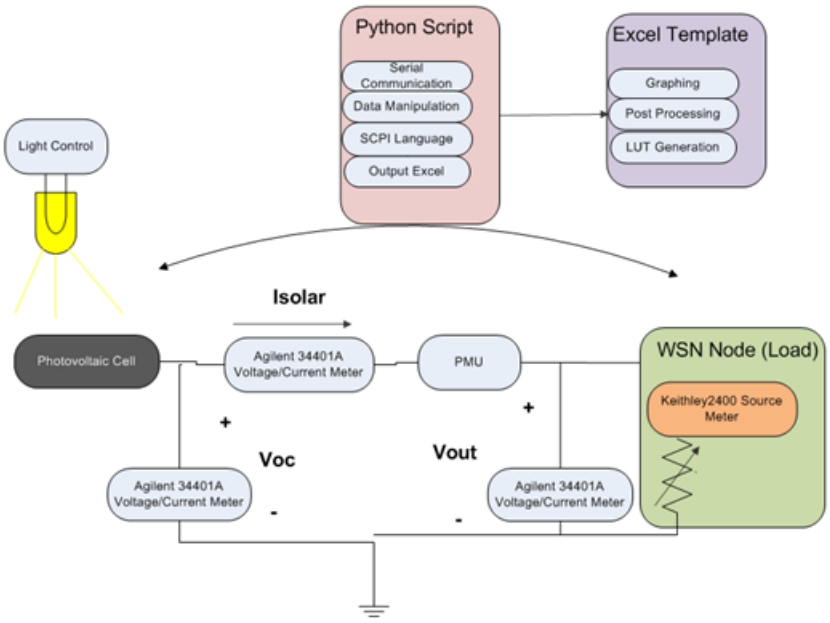

Figure 6.1: The PMU measurement setup is shown. Python scripting is used to provide near real time design feedback.

Creating meaningful I-V and P-V curves requires many data points,

which when gathered manually is extremely time consuming. The slow speed of manual data collection inhibits system design efforts that limits the number of characterization cycles that can be practically performed. To aid in the collection of so much data, an automated lab environment is created to produce rapid results and instant feedback to the design process.

The automation environment is developed around the Python scripting language. Python scripts written pull together communication between the equipment, data manipulation, and logging of results [7] [8]. Communication to the lab equipment is achieved over an RS-232 serial port by sending SCPI commands to the Agilent 34401A multi-meters and the Keithley2400 source meter. The Standard Commands for Programmable Instruments (SCPI) protocol is an industry standard that provides a common language for instruments manufactured from different vendors.

The source-meter acts as a programmable load which can be placed at the output of the stand-alone solar panel or the entire PMU system. It is programmed as a negative current source between -0.03mA and -1mA. The load current is then varied and recorded along with V_{open} and V_{out} into a formatted Excel spreadsheet. This model is effective in creating experimental data in near-realtime. The block diagram illustrating the automation environment is shown in Figure 6.1.

The automated experimental setup did not only provide a convenient way to characterize the system, but it was also the basis characterizing the MESH system. During the development of MESH, the Phyton code [8] was

used to prototype the suitable V_{oper} feedback mechanism. Thus, with the Python script in place, a simple model can be used to simulate MESH in a lab environment without requiring the MSP430 MCU to be connected to the system. The only additions would be a programmable power-supply to emulate the V_{oper} feedback parameter, and Python code implement the LUT. This was done as an intermediate step before introducing the MCU into the equation.

6.2 Solar Panel Quantitative Results

This section contains data and inferences made based on characterizing the performance of the solar panel by itself. These experiments were completed in a controlled environment with a direct source of light as the brightest condition. The light source was consistently varied by counting the number of A4 sized papers placed directly on the light source.

Figure 6.2 shows the solar panel output current I_{solar} dependency on the open circuit voltage V_{open} and the amount of light. The number of paper equates to the amount of light that was shielded from the platform by stacking papers on an incandescent bulb. Higher number of papers imply a darker light setting. Results show that for a given light setting, increasing the voltage on the panel causes the current to degrade. Also, there is a strong dependency on available light and the amount of current the panel produces. Strong light settings produce much higher currents than lower light settings, indicating that there is more available power.

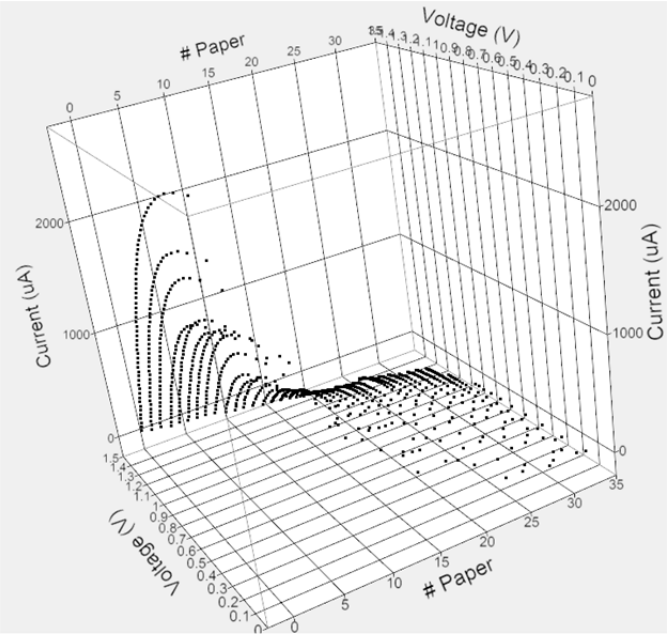

Figure 6.2: V_{open} plotted as a function of PWM I_{solar} and amount of light

Figure 6.3 indicates that the highest current I_{solar} is produced when there is an abundance of available light and the open voltage V_{open} requirements are low. Irrespective, sufficient current is produced when reasonable light conditions are present (less than 7 paper sheets). For example, the target panel voltage of 1V can be met with 1mA even with relatively poor lighting with up to 10 layers of paper on the light.

Figure 6.4 further illustrates the behavior of the solar panel. Raw data was collected and grouped into 5 distinct lighting conditions, each represented by a different color. The plots show that the blue line indicates the best light condition being directly under the light source with little interference. This

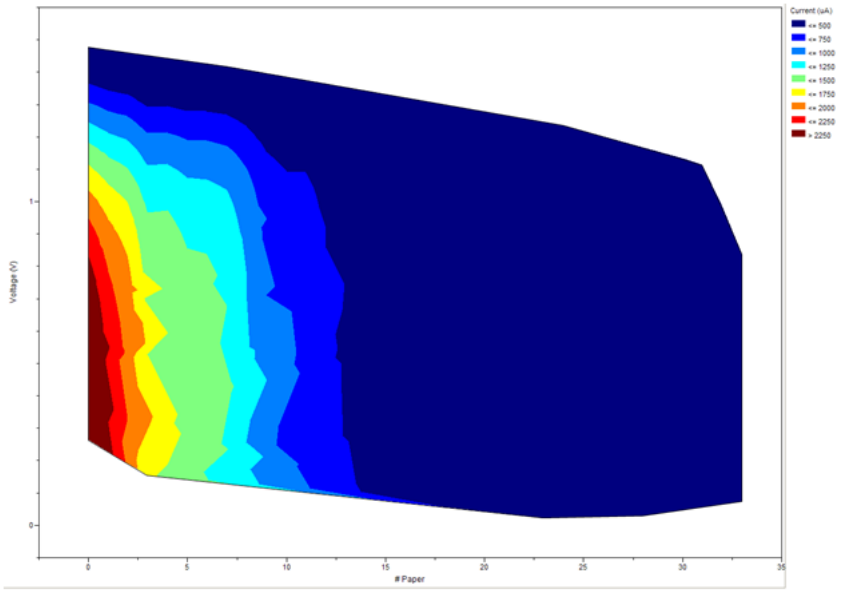

Figure 6.3: Contour plot of I_{solar} as a function of V_{open} and light source. 1V V_{open} can be met with 1mA of I_{solar} even with a relatively low light setting.

group produces the best power for the system, but also assumes a near ideal light condition. The second group in red indicates a more realistic setting and demonstrates the soundness of the system. It indicates that the target of 1V can be met with 1mA of current, which is more than adequate to power the battery, boost converter circuitry, and the overall system. The situation deteriorates quickly when the light source is faint and eventually saturates producing minimal current at 1V (orange plot). The dotted lines represent the power consumption of the solar panel, and is plotted against the I-V plot for reference. Note that the ideal condition exists when there is maximum power transfer. This occurs when the power and current plots overlap each

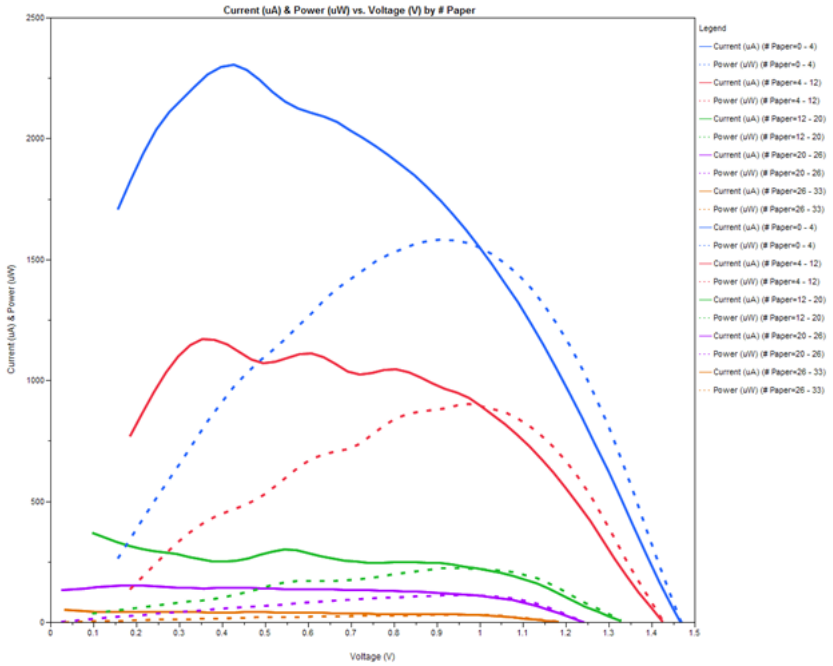

Figure 6.4: Five distinct groups can be formed from the I-V and P-V plots where each group can be considered a power setting that can be later used to optimize the platform.

other.

Figure 6.5 shows all the raw data for all the runs used to compile I-V plots and P-V plots. Notice that the open circuit voltage and the short circuit current can both be deduced from these plots. During the experimentation phase, the true open circuit voltage and short circuit current could not be measured since a sourcemeter was connected as the load of the solar panel. Preliminary results discussed in Chapter 3 show that there is a direct correlation between these two parameters, and that both have a strong correlation

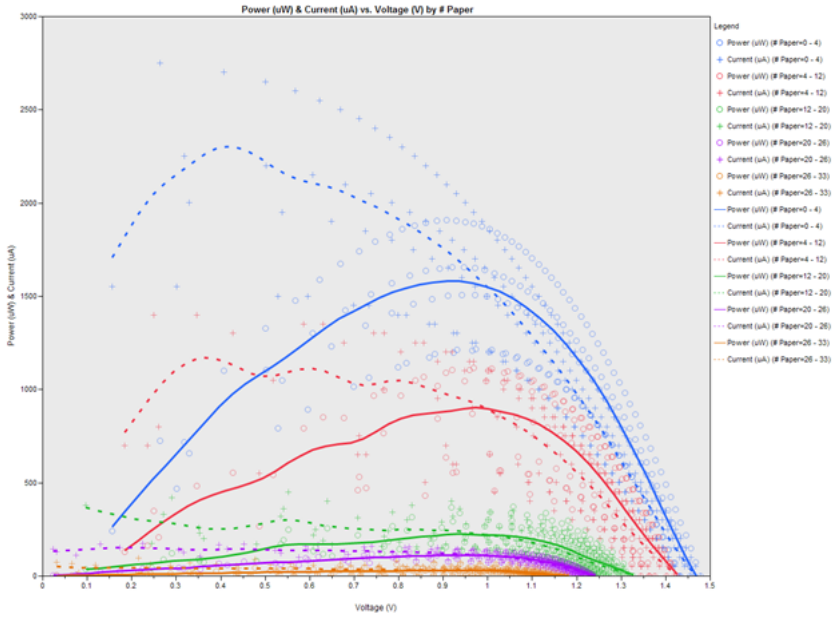

Figure 6.5: Raw experimental data used to compile I-V and P-V plots

to the light intensity and current produced. This correlation can then be used to optimize for the best power transfer or efficiency for the overall platform

6.3 System Level Quantitative Results with CBC5300

This section adds the interaction of the CBC5300 along with the solar panel with varying light conditions. The output load of the CBC5300 is varied with a sourcemeter while voltage and current measurements are obtained in a controlled environment. This setup mimics a real application where the light condition and the source loads are not always known.

Figure 6.6 shows the total system performance with a load for all the

viable light conditions. The top plot shows the efficiency band with varying light conditions applied to the end system. The end systems load in this situation would be the wireless sensor. Because the experiment was in a controlled setup, the best light condition here produces the worst efficiency, since most of the power is thrown away and unused. In this example, the best efficiency is achieved with the lowest light setting. Also notice that the peak efficiency is achieved sooner in a darker conditions compared to a lighter situations. Once, the peak efficiency is achieved, performance deteriorates quickly since the internal regulator is no longer within specifications.

The middle plot in Figure 6.6 discusses the load regulation performance of the overall chip. The plot shows that the best load regulation is achieved with the brightest light condition, since there is ample available power in the system. The results show good load regulation at roughly 3.4V down to approximately 30μA. With more load applied, the performance linearly degrades lower. The final bottom plot in Figure 6.6 shows the solar panel output V_{solar}, which is also the input to the CBC5300 device. The voltage stays at roughly 1V and matches V_{oper} since both of these voltages are inputs to a comparator feedback circuit that matches the voltages. Thus, it is expected that these values match at all times as long as the internal amplifier is in saturation.

Figure 6.7 shows the total system performance with varying V_{oper} for just the maximum light condition. Unlike 6.6, the control that is kept constant here is the light condition, with V_{oper} being varied. Notice that the maximum

efficiency is achieved at the endpoints of V_{oper}, with a toll on the efficiency band. A middle range value selected for V_{oper} shows a wider efficiency band for power transfer, with the toll on maximum efficiency. In an application, if the load is fairly constant, then V_{oper} should be selected to yield the maximum efficiency; in this example, a value of 1V would be selected. However, if the load varies across a wide range, then the goal is to have a wide efficiency band; thus selecting a V_{oper} that is in the middle of the 0.3V to 1.5V range would ensure maximum efficiency for the overall platform.

The middle plot in Figure 6.7 shows the load regulation based on V_{oper}. Results indicate that achieving maximum efficiency takes a toll on the load regulation. Specifically, the load regulation is better when the platform does not achieve maximum efficiency. Hence, the designer must make a tradeoff between maximum efficiency, efficiency band, and load regulation. The best efficiency cannot be chosen in a generic manner. Rather, it highly depends on the load and performance that the application requires. The bottom plot in Figure 6.7 simply confirms that V_{oper} and V_{solar} track, as they are both inputs to an internal feedback amplifier as previously discussed.

Figure 6.8 shows the platform efficiency with varying V_{oper} and output load. I_{src} describes the maximum current that can be pulled from the system for a given condition. In this plot, the light source is held constant at its maximum strength. Results show a dip in efficiency towards the center band of V_{oper}, also seen in Figure 6.9 as well. Notice that the center band around 1V has the lowest efficiency numbers and should be avoided. This also happens

to be the region where the platform operates in by default.

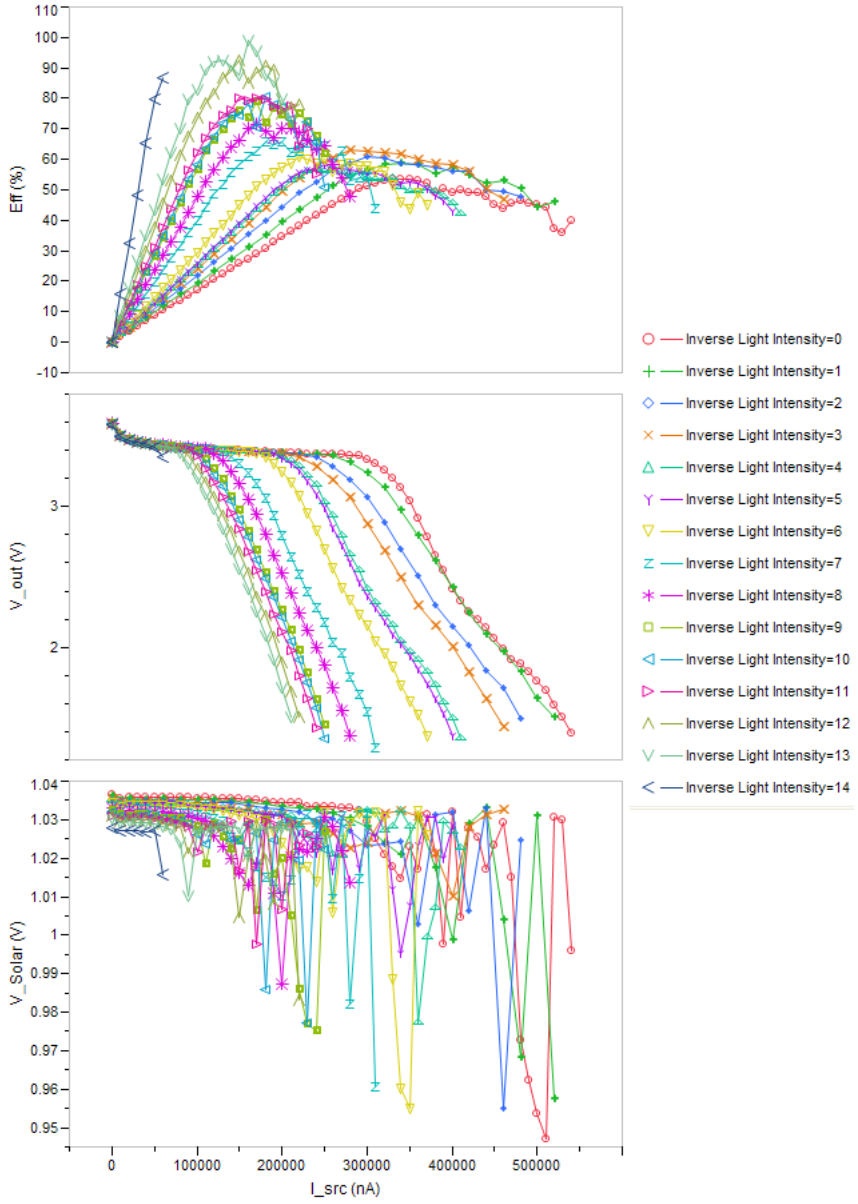

Figure 6.6: Efficiency, V_{out}, V_{oper}, V_{solar} are plotted as a function of the output load I_{src} and light source.

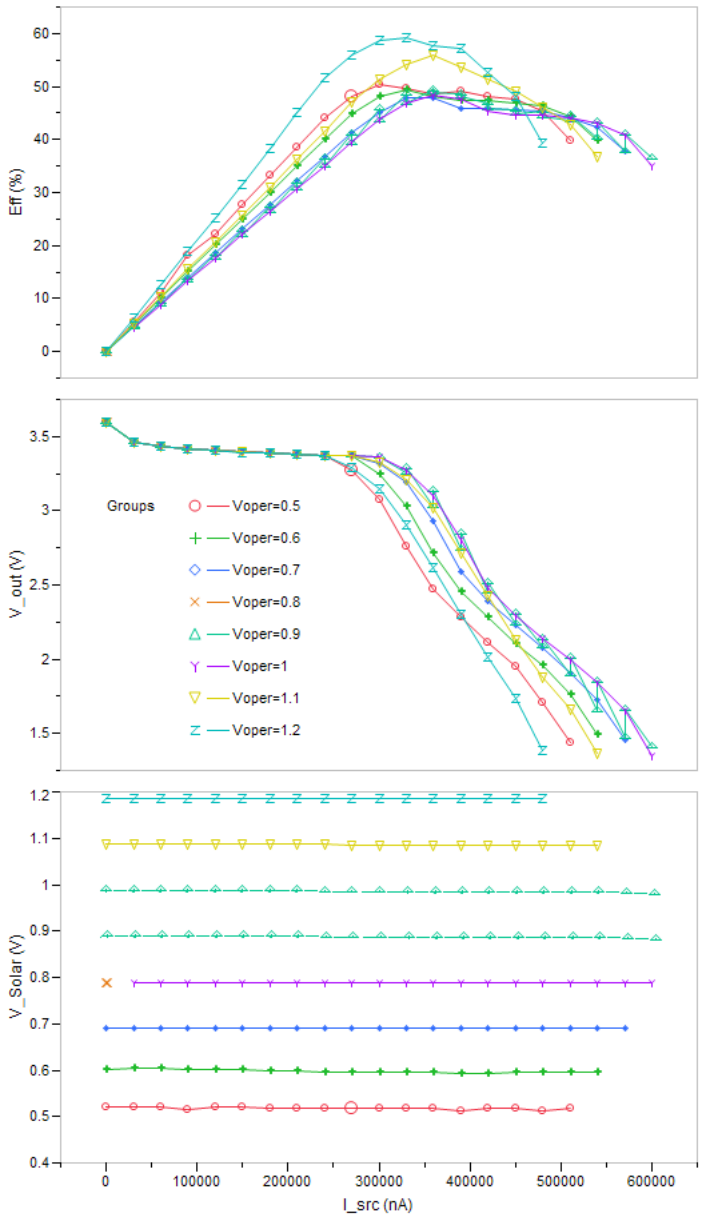

Figure 6.7: Efficiency, and V_{out} shown with varying V_{oper} at maximum light condition.

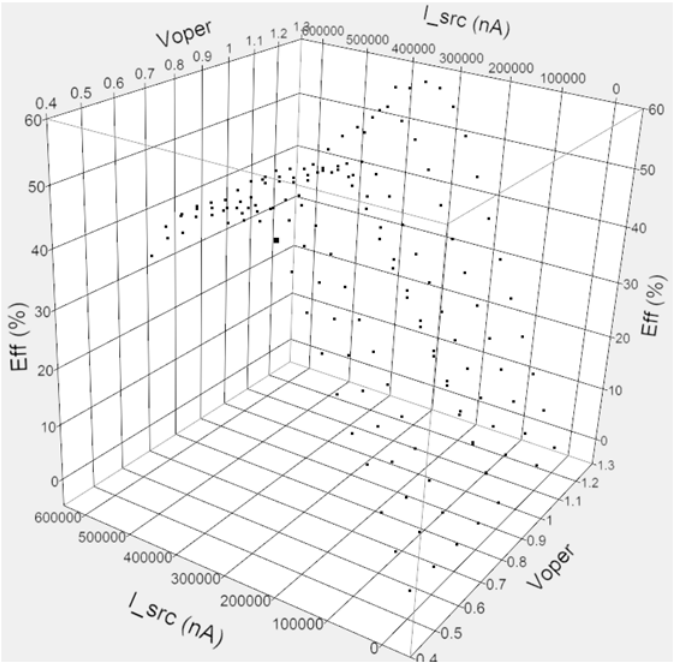

Figure 6.8: Platform efficiency with varying V_{oper} and output load

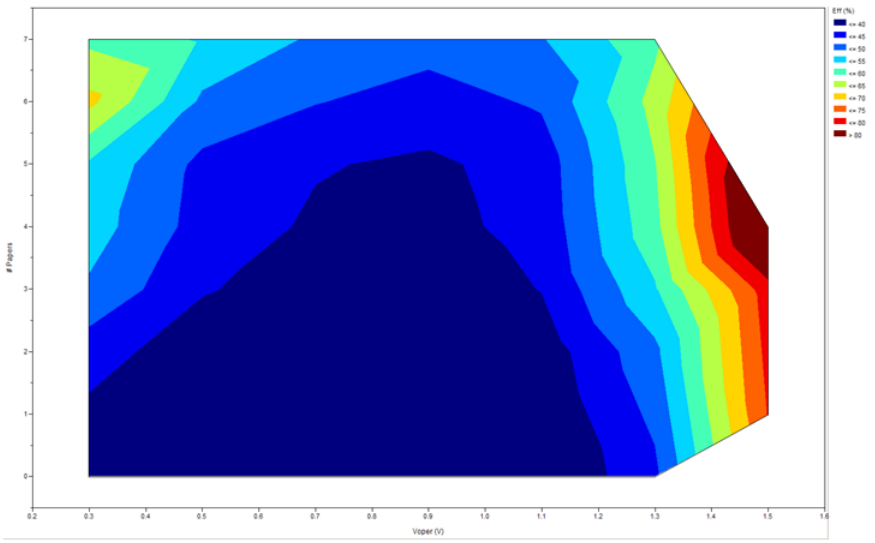

Figure 6.9: Efficiency contour plot showing V_{oper} and varying light conditions.

Chapter 7

Realtime MESH Analysis

This chapter describes real results taken from the TI-RF2500-SEH platform running MESH. After the stand alone platform is fully characterized (Chapter 6), the actual MESH software and hardware additions are proven to be working.

7.1 Realtime MESH Operation

In order to verify that MPPT is being achieved on the platform the individual pieces of MESH are inspected. First, the mechanism that disconnects and reconnects the solar panel is studied. Then, it is determined that actual changes in light intensity are being passed back to the CBC5300 through the PWM duty-cycle adjustments.

Figure 7.1 shows the effect of the GPIO controlling the analog switch (yellow). Whenever the GPIO is high the analog switch is an open, and the load is disconnected from the solar panel. The small picture shows the max frequency of the PWM at which V_{solar} will respond. At some GPIO frequency the analog switch and solar panel are not able to recover, and therefore an upper-limit is determined. The larger picture is a zoomed in instance of the

GPIO going high. Whenever the load is disconnected from the panel V_{solar} will rise since it does not have a load pulling it down. It is at this instance of time that V_{open} is measured by the MCU. Now that the solar panel's disconnection method is verified, the dynamic PWM duty-cycle adjustments are studied.

Figure 7.1: Solar panel is disconnected from the system. The solar panel's voltage (green) rises when the switch (yellow) disconnects it.

The oscilloscope capture in Figure 7.2 shows V_{oper} (and by extension the green V_{solar}) reacting to changing light conditions. As the MESH software runs the PWM is dynamically adjusted. As the light source changes, the MCU that is constantly measuring V_{open} realizes the change and as such adapts by decreasing V_{oper}. This is done by changing the duty cycle on the PWM (yellow). The change in duty cycle then adjusts V_{oper} accordingly. Notice that the duty cycle changes at the midpoint of the oscilloscope capture.

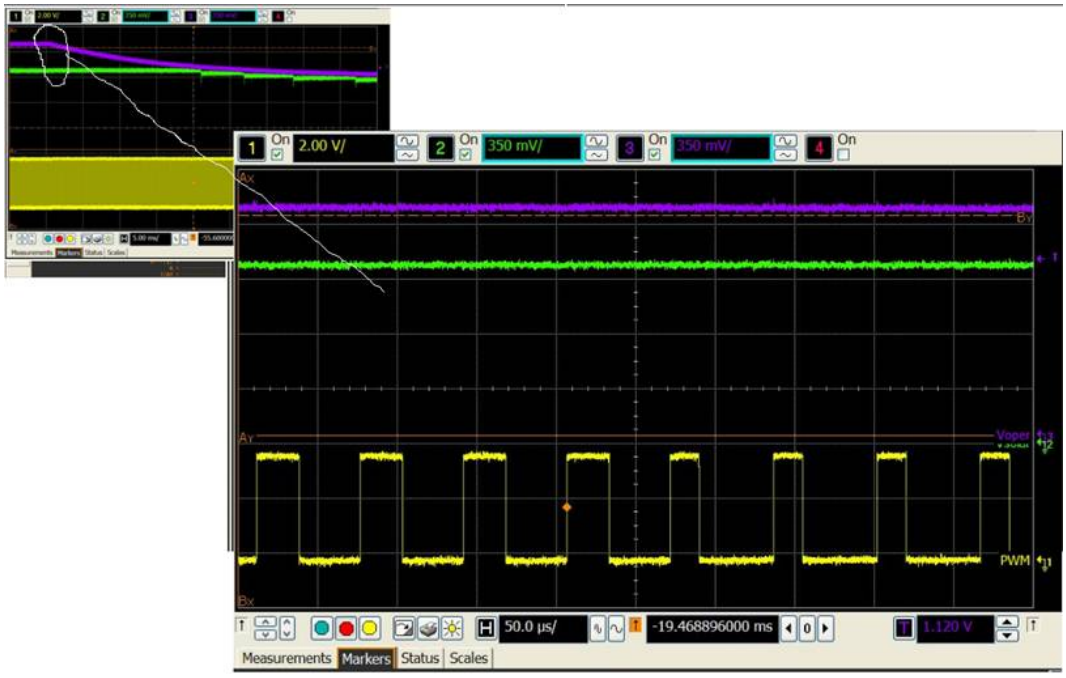

Figure 7.2: PWM duty cycle dynamically adjusts with new LUT value.

Now that the hardware and software components of MESH are validated in the real system, the power consumption of MESH must be considered to ensure an improvement has been made in efficiency.

7.2 Power Breakdown of MESH Components

In order to verify that MESH is a feasible power-saving technique it is important to compare its power overhead to the overall power budget. The power budget is defined as the threshold at which point any additional overhead will outweigh the benefits of adding MESH. This number can be application specific and is best determined by empirical results (Chapter 8). Before

determining if the power consumption of MESH is acceptable the overall system consumption as well as the consumption certain individual components must be understood.

Figure 7.3 shows the current of the complete system while running the WSN demo code without MESH being added. The current is measured by monitoring the voltage across a 50Ω resistor in series with the supply voltage. Every 2.25 seconds four operational modes of the sensor node can be observed. They are: sleep mode (not seen), in steady state mode (lowest bar), waking up to transmit a sequence (middle bar), and then receiving a sequence (highest bar). The device is attempting to connect to the other nodes in the circuit, so sleep time is intentionally minimized. The peak current in this image can be calculated by

$$\frac{1V}{50\Omega} = 20mA \tag{7.1}$$

Figure 7.4 shows the platform current with the addition of MPPT. The first section shows the MCU working in steady state. The sharp dip in current indicates the device is briefly entering into sleep mode to get the ADC measurements (MCU need not be on for ADC to work). Then the device comes out of sleep to set the LUT, drive the PWM, and perform a transmit and receive. Once this mode ends, the device drops in current to a short plateau before reverting to sleep mode. The maximum current here is

$$\frac{1V}{50\Omega} = 20mA \tag{7.2}$$

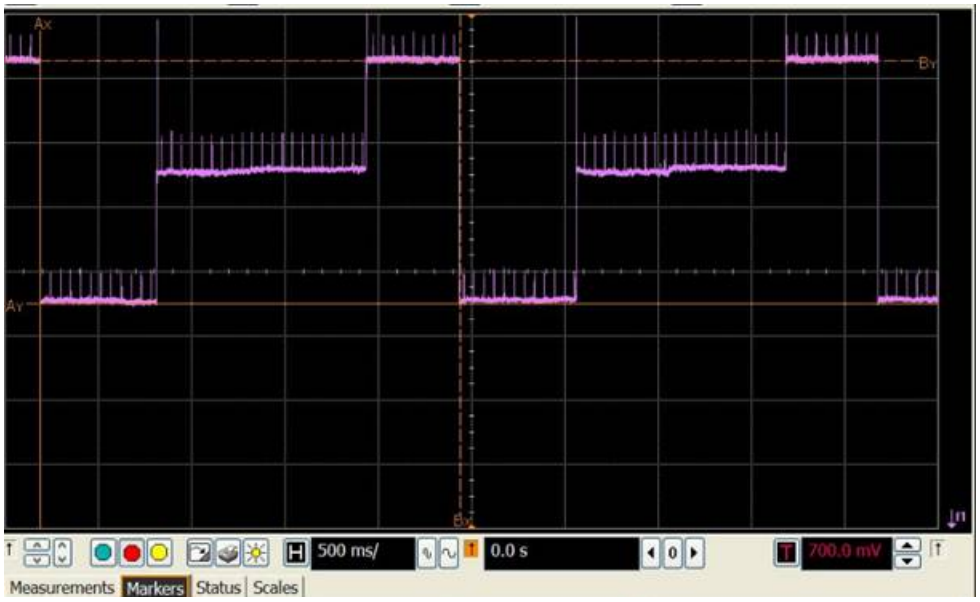

Figure 7.3: Current measurements taken in sleep mode, steady state mode, and wake up sequence.

while in sleep mode the current is

$$\frac{25mV}{50\Omega} = 500mA \tag{7.3}$$

An individual breakdown of hardware and software components of MESH along with their respective power consumptions is shown in Table 7.1.

Table 7.1: MESH Power Breakdown

#	Component	Power	Comments
1	Switch	5 μW	Explained in Chapter 4.2
2	ADC	50 μW	Datasheet
3	PWM	500 μW	MESH experiments
4	CPU LUT	100 μW	CPU calculation

The switch power has been explained in Chapter 4.2. The power burned

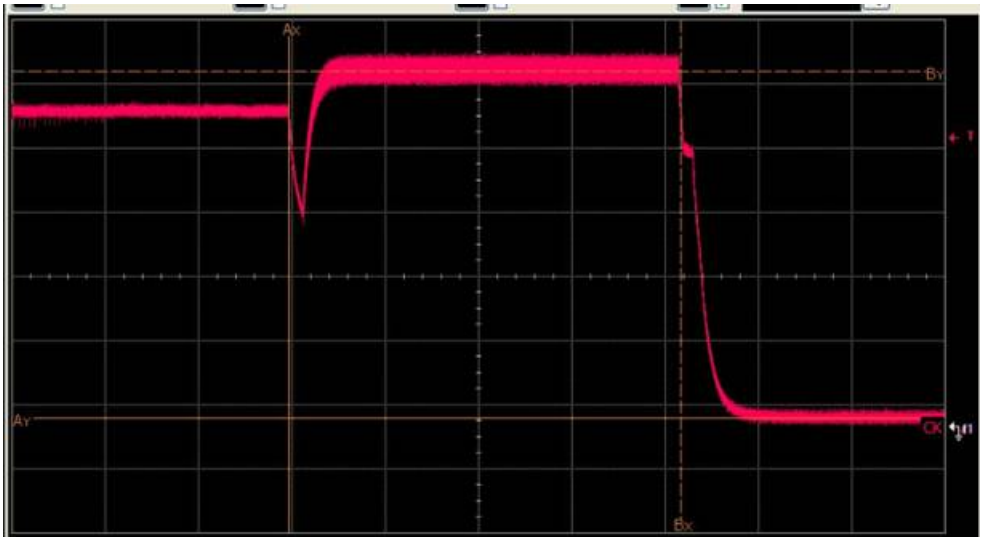

Figure 7.4: Platform current while MESH is being executed

by the switch depends on the current flowing through it. At worst case, it will be roughly 2mA, and the 5μW quoted is calculated based on the worst case scenario. The ADC power is estimated from the [16] and is verified using the MESH setup. The power consumption of this block is a function of how often it is used to measure V_{open}. In this case, a low frequency was chosen to mimic a real-world condition. The PWM shows roughly 200μW being consumed, and is also frequency dependent. Like the ADC setup, a low frequency was chosen for the PWM to optimize power. For MESH, the PWM power is constantly on since it is has to consistently supply V_{oper}. As previously explained, this will eventually be replaced by an internal DAC, which should consume a fraction of the power used by the PWM. CPU LUT cycles is estimated based on MESH integrated into application code. The LUT

calculation is also frequency dependent and is only computed when the LUT must be updated. The total MESH power is then roughly 155μW, which is the value that should be compared to the application specific power budget of the target WSN.

7.3 Noise Analysis of MESH System

In order to collect measurements on the existing platform, modifications had to be made to the solar kit. The end result with the measurement devices connected are shown in Figures 7.5, 7.6, and 7.7.

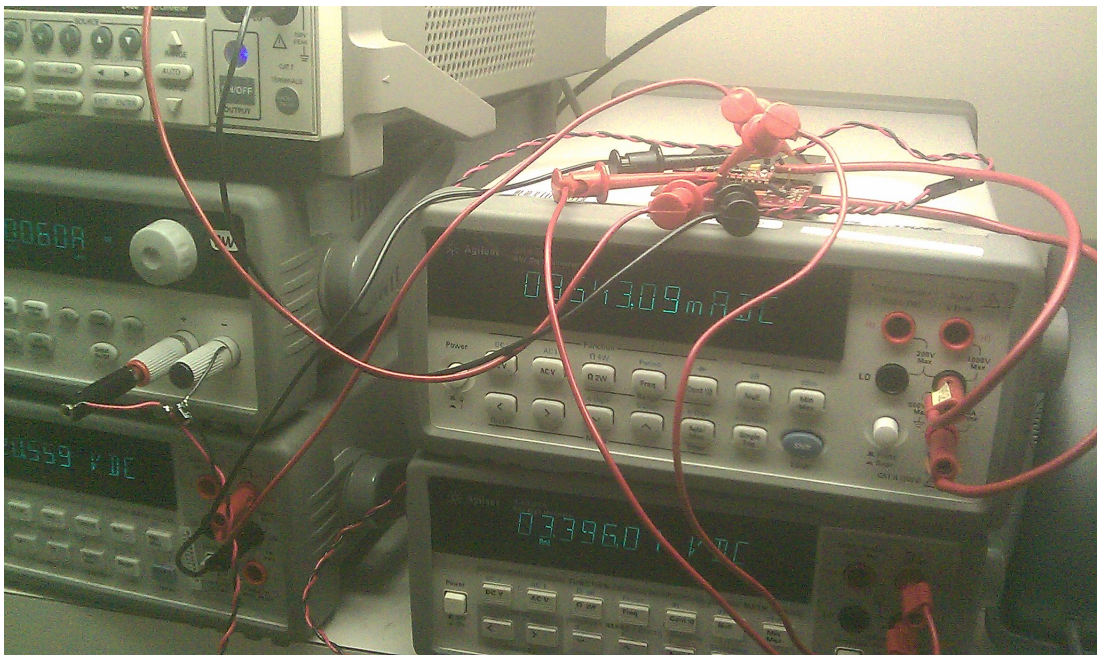

Figure 7.5: Platform shown along with equipment used for measurements.

The modifications include adding hardware to perform the MPPT algo-

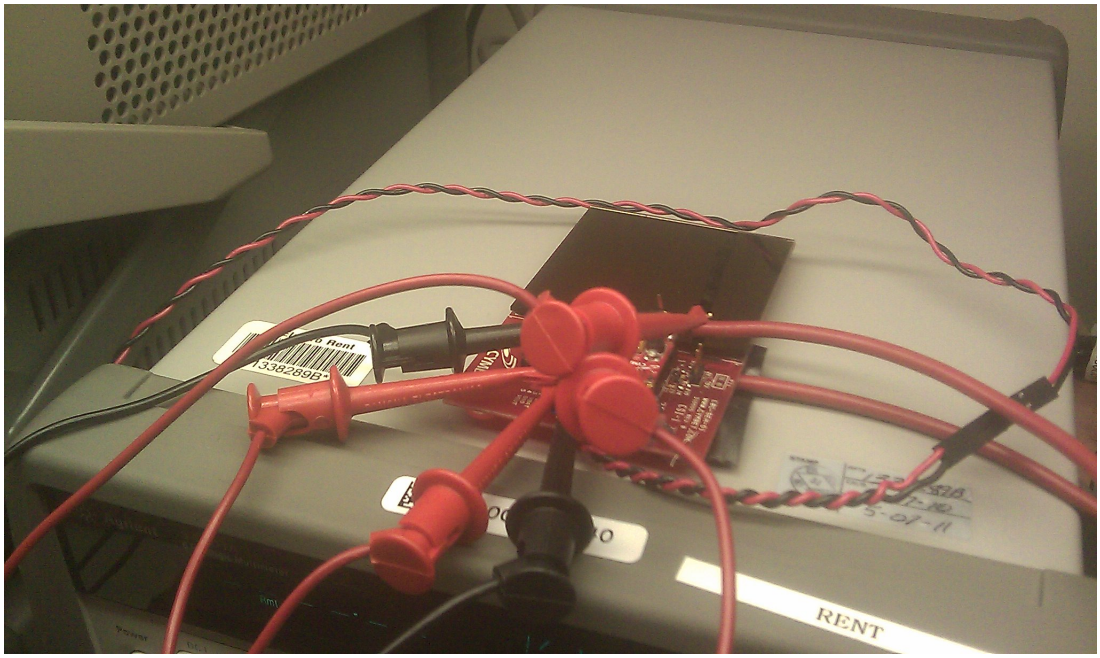

Figure 7.6: Platform measurement connections shown.

rithm and inserting test points where current and voltage measurements could be retrieved. Adding this hardware to an existing platform is not a trivial task since as new connections are run around the printed circuit board (PCB) the ground plane becomes segmented and less than ideal. Efforts were made to consider routing distances and wire gauges in order to minimize these antenna effects and ground loops.

The high-frequency noise seen in the scope plots can be attributed to probing artifacts which exist since some of the measurement instruments and hardware were not on a strong localized ground plane. Because MESH is an addition to an existing platform, its ground references came from thick

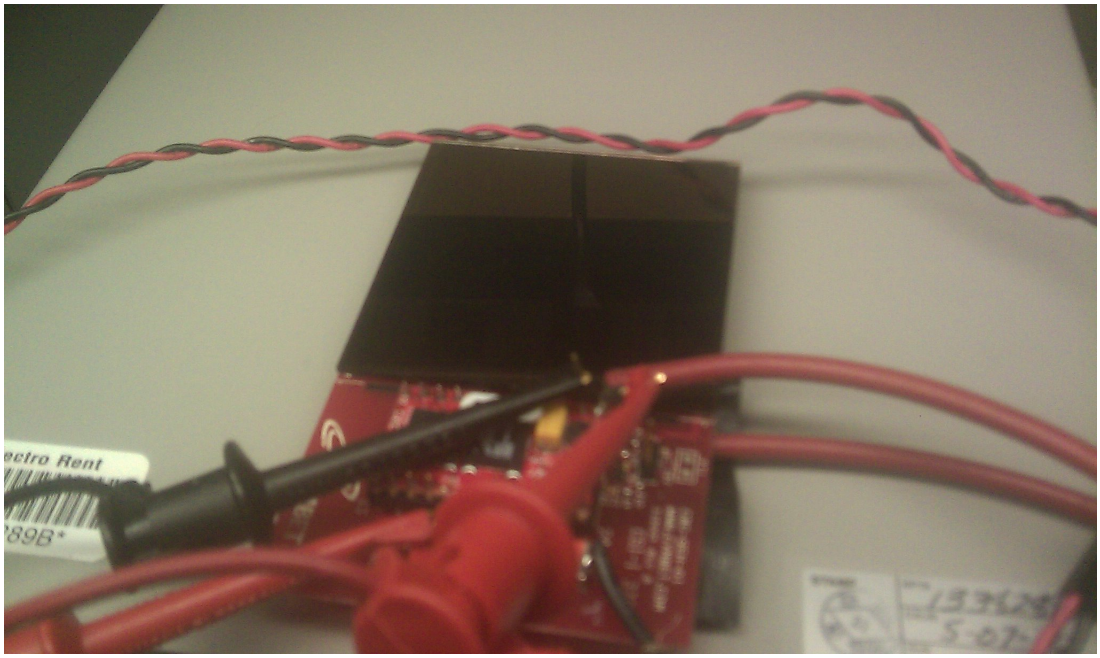

Figure 7.7: Platform connections shown in detail.

wires rather than a solid ground plane on the PCB. Furthermore, the DC-DC converter operates in a relatively noisy environment due to the high switching currents described in Chapter 2. Even though, these factors cause the high-frequency noise seen on the scope plots, they don't necessarily impact the quality of measurements because they are well out of the operating frequency.

Chapter 8

Efficiency Improvements using MESH

This chapter demonstrates the efficiency improvements and power savings realized when MESH is implemented in the TI-RF2500-SEH application example.

8.1 Power Results

The goal of MESH is to improve the conversion efficiency from solar power to available power at the output of the CBC5300. In order to quantify an improvement in efficiency the available output power with and without MESH is compared. This is accomplished by increasing the load of the CBC5300 while the voltage of the load is recorded. At some value of load current the CBC5300 can no longer keep up with the power demand and the output voltage begins to fall. The results of this experiment across multiple light conditions both with and without the presence of MESH is shown in Figure 8.1. The left plot shows the power without MESH, and the right plot shows MESH incorporated. The legend shows the number of papers placed on the light source to block light. In the presence of MESH the available power at the output of the CBC5300 is clearly maximized. The largest improvement is seen at highest

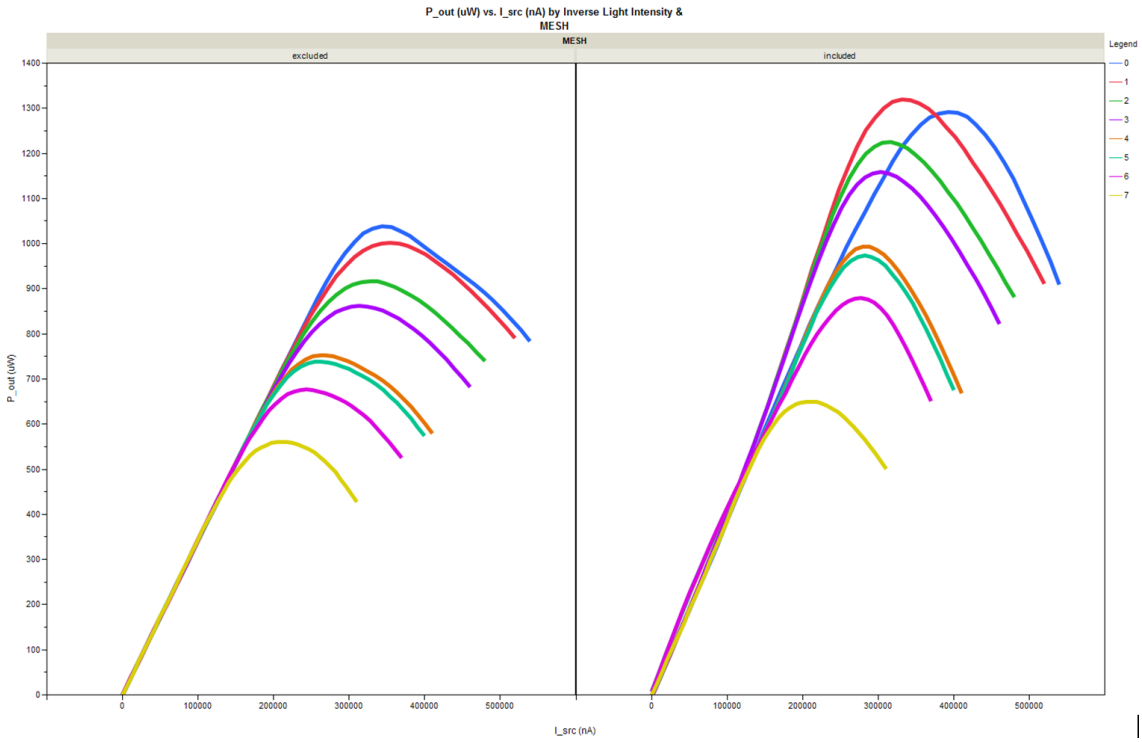

Figure 8.1: Available power measurements with MESH implemented show the greatest improvements when light is most readily available. Lower light conditions also show a considerable gain in available power.

light condition because this where the output impedance of the solar panel is differs most from the input impedance of the CBC5300 with the default V_{oper}. The increase in output capacity allows for higher power consuming applications to be applied downstream from the PMU when light is readily available. All light conditions show a net improvement between 18% and 25% depending on the light condition and current load. This means that the MESH improvement outweighs its power overhead, which was roughly calculated as

155μW.

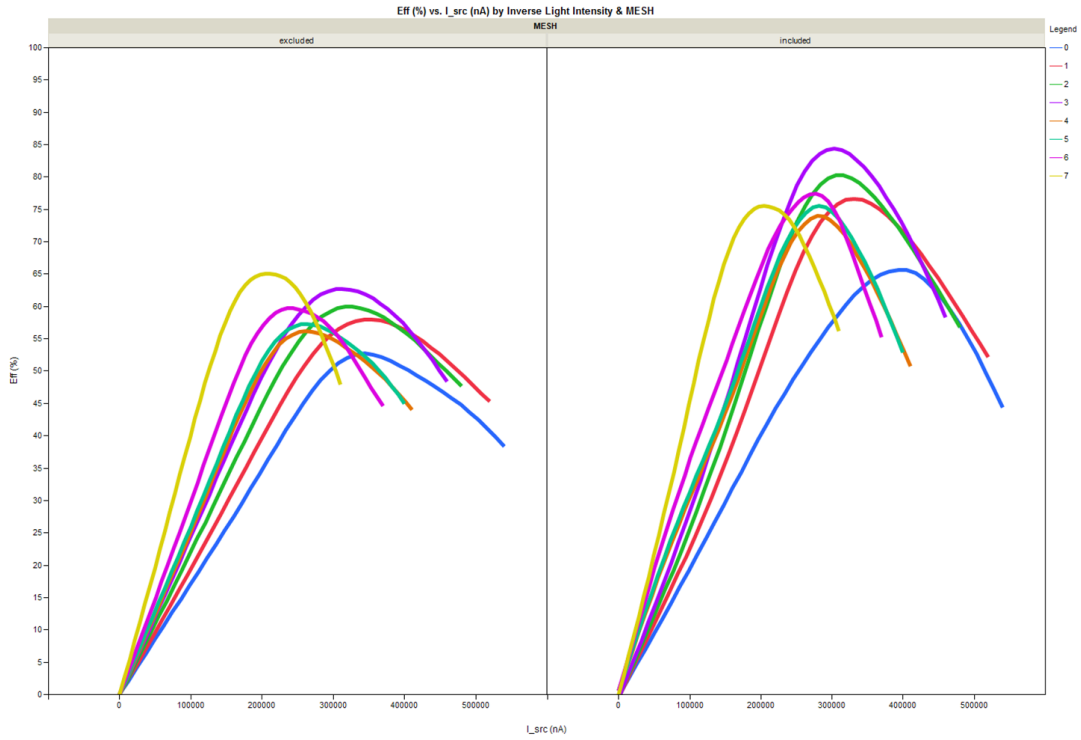

Figure 8.2: Efficiency curves compared for seven light intensities. The addition of MESH has significant efficiency improvements from 18% to 25%.

8.2 Efficiency Results

Like power, PMU efficiency of the CBC5300 has also improved. Figure 8.2 shows that efficiency improvements with the addition of MESH. The input power to the CBC5300 remains fixed for a given light condition since the solar panel is supplying the system. The efficiency has increased if output power of the PMU has increased relative to the input power. Empirical results

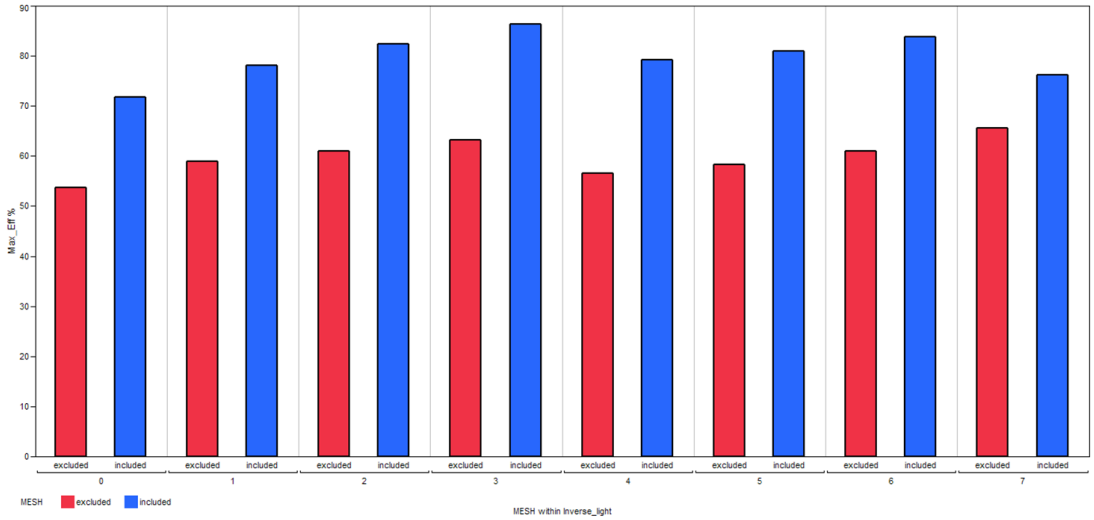

Figure 8.3: Maximum efficiency for each light source level plotted with and without MESH implemented. MESH improves maximum efficiency by an average of 20%.

shown in Figure 8.3 indicate that MESH improves the maximum efficiency of the platform by an average of 20% across all light conditions. The figure shows the seven light intensities with the middle band benefiting the most. This is likely where the platform spends a majority of its time.

Chapter 9

Conclusion

This chapter contains a summary of the project, results reported, and future work.

9.1 Discussion

MESH is an implementation of an MPPT algorithm tuned for a specific solar powered WSN. The hardware and software components of MESH vary the operating point of a sensor node's DC-DC converter based on realtime feedback. This operation actively adjusts the peak power point of the system for various light and load conditions. The operation of MESH can be described in three basic steps. The first step involves actively measuring V_{open}, or the open-circuit voltage of the solar panel. Next, the measurement is referred back to a LUT in the MCU to determine the best operating point for the PMU. Finally, the MCU will drive V_{oper} based on the LUT to ensure maximum power efficiency for the platform.

The LUT can be created by simulation, experiments, or both. The empirical method is chosen because an actual working system was the goal, and simulation models for the complete system is out of the scope of this work.

An automated test suite was used to sweep various parameters to characterize MESH operation before selecting an appropriate values for the LUT.

The resulting MESH is easily implemented in any WSN solution utilizing solar energy harvesting. As a demonstration, MESH is implemented on the TI-RF250-SEH WSN development kit, which accurately models a commercial system. Experimental results of MESH indicate a maximum efficiency improvement of 20% over the native TI RF2500-SEH WSN platform. The implementation resulted in a power overhead of about 155μW, which was less than the additional power gained from using MESH.

9.2 Future Work and Improvements

Existing solar powered WSNs use a variety PMU architectures and solar panels. A procedure will be developed to make MESH more generic so it can be adapted to existing WSN systems. This procedure will include a hardware component selection guide that will provide a metric based on cost and performance. Furthermore, a clear guide for generating LUT values will be constructed for new WSN platforms. These efforts will bolster marketing opportunities for MESH.

An extension to the work on the TI-RF2500-SEH will place several of these MESH enabled devices out in the field so a real application, like that of Joe the Farmer, can be proven. Incorporating many sensor nodes in one study will more accurately show the impact of implementing MESH. New challenges will emerge due to the increased power consumption from network traffic and

the variability of changing light conditions new challenges will emerge.

Bibliography

[1] Digi-Key Corporation. Online Electronic Components Vendor. Available at `http://www.digikey.com`.

[2] Dhople, S.V., Davoudi, A., Nilles, G., Chapman, P.L. Maximum power point tracking feasibility in photovoltaic energy-conversion systems. In *Applied Power Electronics Conference and Exposition (APEC)*, 2010 Twenty-Fifth Annual IEEE , vol., no., pp.2294-2299, 21-25 Feb. 2010

[3] EnerChip EH CBC5300. *Cymbet Corporation*. DC-72-06 Rev06. Available at `http://www.cymbet.com/McontentA/pdfs/DS-72-06.pdf`.

[4] Robert W. Erickson, Fundamentals of Power Electronics. *Springer 2001*, third edition, pages 22–26.

[5] FSA1156, FSA1157 Low-R_{ON} Low-Voltage SPST Analog Switch. *Fairchild Semiconductor*, January 2008. Available at `http://www.fairchildsemi.com/ds/FS%2FFSA1157.pdf`.

[6] S. Kobdish and S. B. Rais. Wireless Sensor Platform. *EE 382-M VLSI Communications*. Spring 2010.

[7] S. Kobdish and S. B. Rais. A Python Script to Characterize the PMU of the TI-RF2500-SEH Wireless Senor. Available at `http://bit.ly/em8NDo`

[8] S. Kobdish and S. B. Rais. A Python Script to Characterize and Simulate a New MPPT Solution for Energy Harvesting. Available at `http://bit.ly/hUABco`

[9] S. Kobdish and S. B. Rais. MESH Software: Wireless Sensor Demo Application With Extensions for an MPPT Solution. *Texas Instruments* Available at `http://bit.ly/f9edmI`

[10] S. B. Rais. *MESH: A Power Management System for a Wireless Sensor Network*. Master's Report, Department of Electrical and Computer Engineering, The University of Texas at Austin, December 2010.

[11] Lopez-Lapena, O. and Penella, M. T. and Gasulla, M. A New MPPT Method for Low-Power Solar Energy Harvesting. In *Industrial Electronics, IEEE Transactions*, September 2010, vol. 57, no. 9, pages 3129–3138.

[12] Peng Wang, Haipeng Zhu, Weixiang Shen, Fook Hoong Choo, Poh Chiang Loh, Kuan Khoon Tan, A novel approach of maximizing energy harvesting in photovoltaic systems based on bisection search theorem. In *Applied Power Electronics Conference and Exposition (APEC)*, 2010 Twenty-Fifth Annual IEEE , vol., no., pp.2143-2148, 21-25 Feb. 2010.

[13] Sensor Expo 2001. `/www.sensorsexpo.com/`.

[14] Simjee, F.I., Chou, P.H., Efficient Charging of Supercapacitors for Extended Lifetime of Wireless Sensor Nodes. In *Power Electronics, IEEE*

Transactions, vol.23, no.3, pp.1526-1536, May 2008.

[15] 5571: 8-Bit Digital-to-Analog Converter. *Texas Instruments*. August 2005. Available at `focus.ti.com/lit/ds/symlink/dac5571.pdf`.

[16] MSP430x1xx Family: User's Guide. *Texas Instruments.* Availabble at `http://focus.ti.com/lit/ug/slau049f/slau049f.pdf`

[17] eZ430-RF2500-SEH Solar Energy Harvesting Development Tool: User Guide. *Texas Instruments.* Available at `www.ed-china.com/ARTICLE_IMAGES/200903/20090304_PM_POW_TS_99.PDF?SOURCES=DOWNLOAD`

Vita

Stephen Kobdish was born in Austin, TX. He is the son of Mark Kobdish and Laura Judd. He received a Bachelor of Science degree in Electrical Engineering from University of Texas at Austin. He then worked as a hardware application engineer at SigmaTel before joining Intel Corporation as a analog validation engineer.

Permanent address: 2130 Saratoga Dr.
Austin, TX 78733

This report was typeset with LaTeX† by the author.

†LaTeX is a document preparation system developed by Leslie Lamport as a special version of Donald Knuth's TeX Program.